Copyright 2014 David M. Friday

IN PURSUIT OF A CHEMICAL AND PHENOMENOLOGICAL UNDERSTANDING OF LONG-LIVING ATMOSPHERIC PRESSURE WATER-BASED BALL PLASMOIDS

BY

DAVID MARK FRIDAY

THESIS

Submitted in partial fulfillment of the requirements
for the degree of Master of Science in Chemistry
in the Graduate College of the
University of Illinois at Urbana-Champaign, 2014

Urbana, Illinois

Adviser:

Associate Professor Benjamin J. McCall

ABSTRACT

Atmospheric pressure water-based plasmoids have been studied for over a decade now, however a large amount of information regarding how the plasmoid is impacted by the parameters of the plasmoid generator and environment, and what chemical species are present in the plasmoid has not been reported. To fill this gap, the geometry and the materials of the plasmoid generator were varied greatly in order to determine how the plasmoid changes in response to each of these parameters. Furthermore, the effect the atmosphere's and environment's parameters have on the rising plasmoid was studied in a controlled environment. Mass spectrometry of these plasmoids was also performed using an ion trap and an orbitrap in order to identify the ions present in the plasmoid. These spectra revealed the presence of $(H_2O)_nH^+$ (n=2, 3), $(H_2O)_nNO^+$ (n=0, 1), and several small molecules including H_2O, NH_3, and NO_3 bound to metal ions. Using isotopic labeling, these ions provided quantitative evidence showing the plasmoid's unique ability to protect its contents from mixing with the ambient air.

To the Creator of these mysteries, and my wonderful families,

both in Peoria and at Stratford Park Bible Chapel

ACKNOWLEDGMENTS

To begin, although the work contained in this thesis was completed in 18 months, it would not have begun without the guidance and assistance of LtCol Brian Tom, Capt Jeremiah Betz, and especially Dr. Mike Lindsay who all developed the original plasmoid generator used in these experiments and who have encouraged me in my attempts to understand this phenomenon. Also, I would like to thank the US Air Force Academy's Department of Chemistry for allowing me to pursue this work.

My time here at UIUC has been an incredible learning experience, largely because of Prof Ben McCall and his continuous flow of encouragement, patience, and guidance as I've sought to better understand this phenomenon. I am very grateful for his adventurous spirit and his willingness to take me on with a new project and only ~18 months to work. Despite this short time frame, I have learned so much about how to do this thing called "research" well from his allowing me to pursue whatever prize I chose to pursue, but refocussing me when I had gotten sufficiently lost.

I would also like to thank the entire McCall group for their patience and help with this new Air Force guy. I've appreciated all your patience, scientific discussions helping me refocus on the big picture of my experiment, and distractions to help get my mind get out of infinite loops. Also, I would like to thank my undergraduate assistant Zhangji Zhao, whose help and skill at problem solving and has been invaluable in enabling me to pursue the wide variety of experiments reported here.

I am extremely grateful to Prof. Richard Perry for graciously providing the expertise, equipment, and opportunity to take the mass spectra that were so central to this work. Both he

and his students, especially Kevin Peters and Heather Robison, provided generous amounts of time preparing for these experiments and technical assistance and instruction in working the spectrometer and analyzing the spectra. I'd also like to thank Prof Thomas Dolan for making time for our discussions about chemical reactions in plasmas and his interest and suggestions for this work.

Lastly, I'd like to thank my Lord, Jesus Christ and His Holy Spirit for being my sustainer while I've been here at UIUC, as He's been for the past 23 years. I am infinitely and eternally indebted to Him for His unconditional love for me and forgiveness of all my failings which have become all the more obvious here in grad school. Also, I'm grateful that He created this phenomenon, if only to put me in my place; I've appreciated the challenge. And to God, my Father, thank you for working Your plans in me, reconciling me to Yourself as a son, and providing this opportunity to learn and serve You here at UIUC.

TABLE OF CONTENTS

CHAPTER 1: INTRODUCTION

Water-based atmospheric pressure ball plasmoids are a fascinating and intriguing phenomenon first observed by Egorov and Stephanov in 2002 [1]. Produced with only a high voltage power supply, capacitor, two simple electrodes and a container of water, these plasmoids are extraordinary in two ways. First, they emit light for a total of over 400 ms given a pulse of high-voltage DC electricity that provides appreciable current for only ~200 ms. This long lifetime is unprecedented in the laboratory at atmospheric pressures without a fuel source. Reported "long-lived" plasma afterglows include lifetimes of ~1 ms in a 4 torr Ar-Hg mixture [2], and two papers modeling atmospheric air afterglows (T_e = 2 eV and 7.5 eV, $n_e = 10^{16}$ cm^{-3} and 10^{12} cm^{-3}, in [3] and [4] respectively) show that nearly all chemical reactions cease in <1 ms. Secondly, these plasmoids are self-contained, showing a clear and nearly spherical boundary between the plasmoid and the surrounding environment. As reviewed in [5], DC-generated atmospheric pressure plasmas are confined to traveling between two electrodes as an arc, corona, glow discharge, dielectric barrier discharge, unless the plasma is blown out from between the two electrodes, typically in a turbulent fashion. Recently plasma sources capable of producing laminar jets of plasma capable of shooting plasma 550 mm have been produced with high velocities (1000 m/s) [6]. However, to the author's knowledge, these ball plasmoids are the only laminar low-velocity plasma-based phenomenon not confined between electrodes to be reported.

Partially due to the simplicity of the experiment, this captivating phenomenon has been studied by many scientists around globe. The following pages give a thorough summary of the research on atmospheric pressure ball plasmoids to date. Since this summary uses some

terminology and equipment described in Chapter 2, it may be helpful to read the description of the plasmoid generator in Chapter 2 first.

Effects of the Plasmoid Generator on the Plasmoid

A very thorough, step-by-step description of how the plasmoid forms is described in [7] and [8], revealing that first streamers quickly shoot out over the surface of the water, followed by a collection of plasma into a slowly rising ball above the central electrode which eventually completely separates itself from the electrode. The effect of the plasmoid generator's voltage, capacitance, and conductivity on the lifetime of a plasmoid has been reported by Friday et al. [9]. These results showed how the voltage, capacitance, and resistance each affect the lifetime of the plasmoid, as well as how deviating the pH of the solution from neutral can marginally improve the lifetime of the plasmoid. The diameter and lifetime of the plasmoid were both fit to a function of total input energy ($E_{pulse} = \int_0^{t_{pulse}} I \cdot V dt$) and capacitance [7].

$$\text{Plasmoid Diameter} \propto C^{1/2} \cdot E_{pulse}$$

$$\text{Plasmoid Lifetime} \propto C^{1/3} \cdot E_{pulse}{}^{2/3}$$

The importance of the central electrode being the cathode was first mentioned by Egorov et al. [10] and confirmed by other groups. Less thoroughly reported observations include that the shape and lifetime of a plasmoid degrade as successive plasmoids are produced over a single solution of water [11]; lasers can deform the plasma [12]; and increasing the humidity of the ambient air increases the lifetime of the plasmoid [13].

Fantz et al. performed a thorough analysis of the electrical discharge itself, showing that the total energy used in the production of the plasmoid has a relatively simple formula [14].

$$E_{pulse} = \frac{C\,V_0^2}{2}\left(1 - \exp\left(-\frac{2A_{eff}\,t_{pulse}\,\sigma_{water}}{C\,h_{re}}\right)\right)$$

It was also shown that if one assumes that the resistance of the bucket is constant, less than 25% of the energy in the discharge is used in the production of the plasmoid, the remaining energy being lost to ohmic heating in the aqueous solution.

Plasmoid Physical Properties

There is some disagreement in the literature regarding the physical properties of the plasmoid. Based on the velocity of the plasmoid, Egorov et al. concluded that the plasmoid must be < 330 K [1] [15]. Placing a 0.2 mm diameter wire with a melting point of 475 K into the plasmoid at 15 cm, the height of the plasmoid at 100 ms, did not produce any melting, potentially indicating a temperature < 475 K [12]. However, thermocouple measurements reported in [16] showed that the gas temperature is 600 K at 260 ms, 900 K at 235 ms, and probably > 1300 K at < 200 ms. It has been shown that the plasmoid typically cannot burn through paper; however, this may be due to a cooler boundary layer around the plasmoid [16]. Schlieren imaging did reveal a ~1 cm transitional boundary between the dense air and the less dense plasmoid interior [9]. In contrast, the plasmoid did combine more rapidly on a metal surface, producing sputtering in the process [10].

There is also some disagreement in the literature regarding the density of the plasmoid. From the upward acceleration of the ball in the Schlieren videos, the plasmoid's density was found to be ~66% of that of ambient air, assuming no viscous effects [9]. However, laser beam deflection measurements taken as the plasmoid rose through the beam indicated that the plasmoid's density was ~13% of air, assuming a spherical ball [17]. Using the ideal gas law, these densities would correspond to temperatures of 430 K and 2200 K respectively.

The net charge carried by the plasmoid is reported as being more than -10^{-7} C by integrating the current observed using an antenna dipole in [18], -10^{-8} C using a Faraday cylinder

in [15], and below 10^{-10} C in [16]. All three sources, however did report that there were charged bilayers on the surface of the plasmoid, or possibly within the ball. Those who reported a net charge on the plasmoid explicitly claimed that these bilayers are a collection of negative charges on the surface of the ball followed by an uncharged region between the surface of the ball and plasma inside. When current was still flowing from the central electrode, the floating potential was found to be > ±200 V [16], the sign depending on the polarity of the central electrode, and > -500 V [15]. After the capacitors were disconnected from the central electrode, the floating potential dropped to 0.5 V at 250 ms and 0.05 V at 600 ms [16]. It was observed that the plasmoid stretched and died much faster in the presence of a horizontal E-field [1], and that the plasmoid had no appreciable magnetic fields [16].

Plasmoid Chemical Properties

The most revealing insights as to what chemical species are present in the plasmoid have come from the UV-vis spectroscopic study performed by Versteegh et al. [16]. Aside from several Na(I), Ca(I), Cu(I), Ca(II), and H emission lines at early lifetimes, the emission spectrum primarily consisted of CaOH emissions at 75 ms, and notable OH emissions at 135 ms. The strongest Cu and Ca lines were optically thick, showing reversal, presumably due to absorption in the boundary layer. From Stark broadening of Cu(I) line, the electron density was found to be 10^{16} cm^{-3} at 10 ms and 10^{14} cm^{-3} at 75 ms. The electron temperature was found to be 5000 K at 0 ms, 3000 K at 75 ms, and 2500 K at 225 ms using a pair of Ca(I) lines. These temperatures agreed well with the temperature of 0.3 eV (3500 K) reported by Wurden et al. using the H_α and H_β lines [19]. The OH rotational temperature was found to be non-thermal, having a temperature of ~10^4 K at J>7 and ~10^3 K at J<7; this non-thermal distribution is similar to that produced by the dissociative excitation of water vapor (described in [16]). From these observations Versteegh

et al. proposed that the dissociation of water stores the energy necessary for long-term emission by forming H_2, O_2, or H_2O_2 from OH at the boundary layer of the plasmoid.

Other insights into the chemical nature of the plasmoid are that 0.01 g of H_2O was typically evaporated each trial [14]; many small particles, between several μm and < 200 nm were observed, the larger of which contained the tungsten, the electrode material [8]; and it was reported that soft X-rays were produced by the plasmoid [11].

CHAPTER 2: THE PLASMOID GENERATOR

The plasmoid generator used in this thesis produced plasmoids via a high voltage (+4-10 kV) high capacitance (225-1958 μF) electrical discharge from an aqueous solution, through air, to a grounded electrode ~2 mm above the surface of the aqueous solution. Diagrams describing all parts of the plasmoid generator are shown in Figures 2.1 and 2.2.

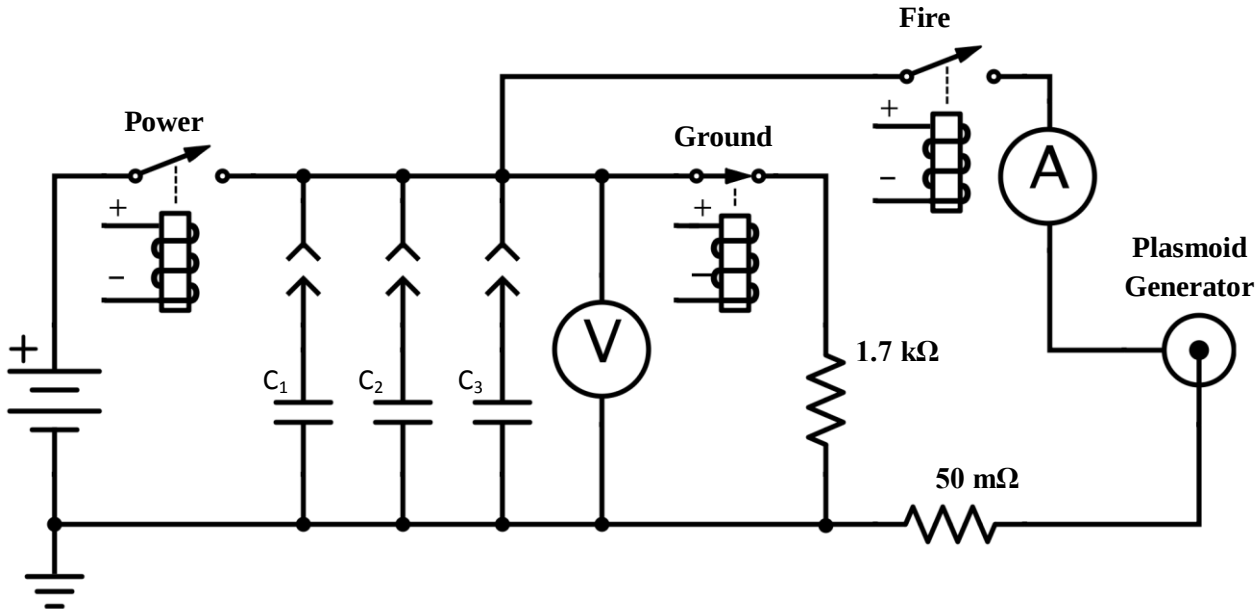

Figure 2.1 An electrical diagram of the plasma generator. $C_1 = 873$ μF, $C_2 = 860$ μF, $C_3 = 225$ μF

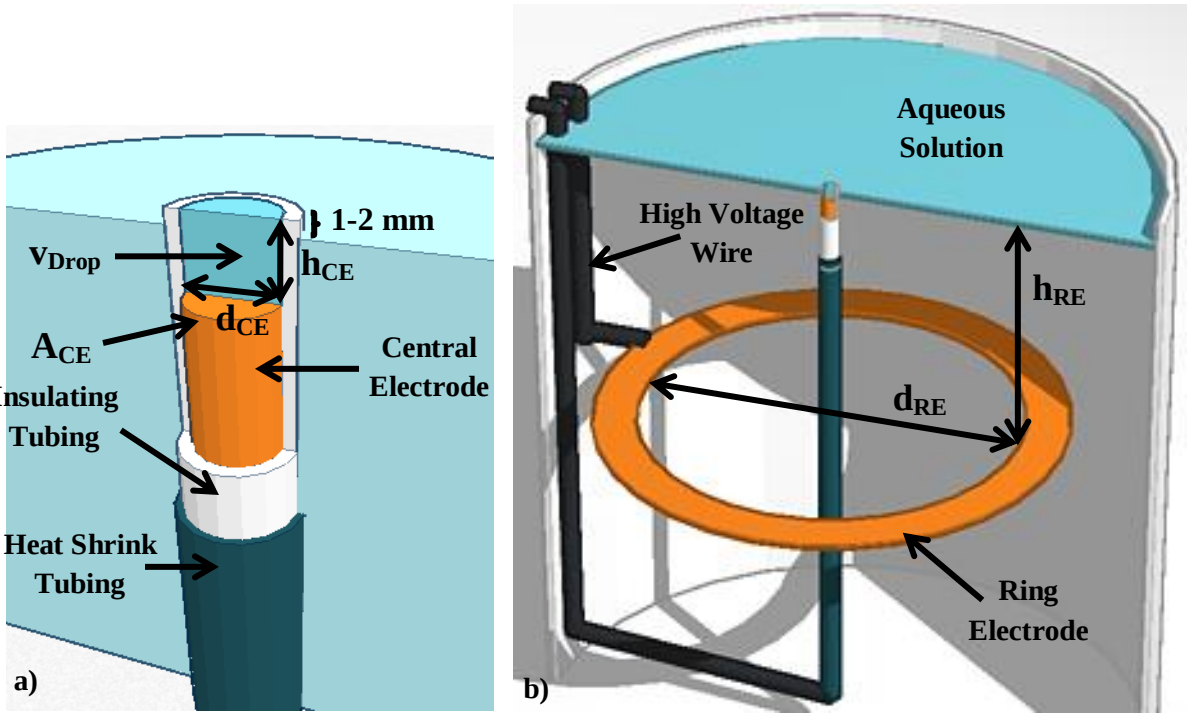

Figure 2.2 The plasmoid generator. a) A close up view of the central electrode and its surrounding parts with the insulating tubing partially cut away. b) The full plasma generator with a cut away of the container and the aqueous solution removed.

The HV capacitors can be used individually or connected in parallel, summing their capacitances. The charging and grounding of the capacitors is controlled by a series of HV relays in air which are controlled by an Arduino microcontroller. The relay that supplies current to the plasmoid generator is in a container filled with "Alpha-1" dielectric oil to restrict arcing across the relay to < 100 ms. These relays have a 50 ms operate time, and do not break current well, as they are only capable of cutting 2.3 A at 2 kV when fully open in oil. However, they are sufficient for tests that are not concerned with the discharge pulse length (t_{pulse}).

For diagnostics, the voltage and current are measured with a voltage divider and a Hall-effect current sensor using the same microcontroller. The humidity and temperature of the air around the plasma generator are also monitored by the same microcontroller. Lastly, video of the plasmoid was recorded with a Pixelink® PL-B742U video camera capable of taking up to

100 fps. From these videos, the lifetime was determined by measuring the number of frames from the first light of the discharge to the last light of the ball-plasmoid. This method could produce ~20 ms of variability depending on the video's exposure time, aperture, camera distance, etc. The plasmoid velocity was measured as the velocity of the highest point on the plasmoid until the upper sharp boundary disappeared.

The central electrode consists of a ~5 cm long electrode with diameter d_{CE} (6 - 10 mm) and an area $A_{CE} = (\frac{\pi}{4} \cdot d_{CE}^2)$ placed inside an electrically insulating tube with a large dielectric strength. These tubes are ~4 cm long and have inner diameters equal to d_{CE} and thicknesses of ~1 mm. The electrode is held at a specific depth (h_{CE}) inside the insulating tube, varying from 15 to -6 mm. A negative depth indicates that the electrode extends above the surface of the insulating tube. If the depth of the electrode (h_{CE}) is less than 0 mm, a small amount of water (v_{drop}) with conductivity (σ_{drop}), typically from the aqueous solution, can be pipetted to the surface of the electrode to reduce the air gap between the electrode and the surface of the grounded aqueous solution. Furthermore, the top of the insulating tube is consistently held at 1 - 2 mm above the surface of the aqueous solution. This reduces the air gap between the electrode and the surface of the water, ensuring a dielectric breakdown of air can occur, forming plasma. The bottom of the electrode is connected to the HV relays via HV wire and an electrical bus surrounded by heat shrink tubing and sealed with electrical tape.

The aqueous solution can contain any one of a variety of electrolytes (salts or acids), giving the solution a conductivity (σ_{water}) ranging from 40-1500 μS cm^{-1}. Also inside the electrolyte solution is a copper ring electrode with diameter, d_{RE}, centered on the central electrode and depth, h_{RE}, from the surface of the water. The aqueous solution is contained inside

either a 5-gallon bucket or a custom made bowl (described in Section 2.2) if a minimal amount of the aqueous solution was required.

2.1 Materials Tested

The Central Electrode

The ideal central electrode should be highly conductive since it may carry > 100 A, and have a high thermal stability since it will be exposed to temperatures > 2000 K [16]. Additionally, the central electrode can either assist or hurt plasma diagnostics by emitting small particles into the plasmoid. To accomplish these goals, several materials were tested, as summarized in Table 2.1.

Material	Advantages	Disadvantages
Graphite	- Conductive non-metal	- Produces orange splotches in the plasmoid due to burning - Introduces complicated organic impurities into the plasmoid
Aluminum	- Releases small particles (presumably Al_2O_3) which scatter light, showing the movement of the air around the plasma	- Melts, rusts, and sputters easily - Al is hard to ID in MS because it is monoisotopic
Stainless Steel	- Fairly strong and resistant to melting - Can produce red pathlines in the plasma if rusted, aiding visualization after the bulk of the plasma had darkened	- Contains several elements, complicating MS - Slowly rusts and sputters
Copper	- Contains 1 element with 2 common isotopes, making it identifiable via MS - Allows for identification of small molecules by MS via clustering - Easily machinable, but robust - Produces no visible changes in plasmoid	- Slowly burns and sputters, but it does not seem to affect the plasmoid.
Tungsten	- Very robust material, no rusting sputtering or melting - Not detectable with MS or visually	-Very difficult to cut or machine

Table 2.1 Materials tested as central electrodes

It should be noted that electrical discharges from metal electrodes in water were studied in [20] and it was found that certain metals can produce dielectric breakdown at lower voltages. For example, if a lower-voltage discharge were desired, a nickel electrode would be much more effective than a copper electrode.

The Insulating Tube

When a plasmoid is produced, the insulating tube is placed under high electrical stress (produced by the electrical fields), thermal stress (> 2000 K) [16], and potential mechanical stress (produced by thermal expansion of the tightly fitting electrode). Therefore, the insulating material must be chosen well, depending on the conditions of the discharge. The advantages and disadvantages of each type of insulation tested are summarized in Table 2.2.

Material	Advantages	Disadvantages
Mylar® (3-200 μm layers)	- Flexible	- Burns completely in a single trial at 4 kV
Macor® (46% SiO_2, 17% MgO, 16% Al_2O_3, 10% K_2O, 7% B_2O_3, and 4% F)	- Machinable ceramic - Only insulation that survives discharges at > 7-9$^+$ kV - Slowly melts, instead of breaking	- Introduces diverse impurities into the plasma detectable via MS and visible in video if ≥ 5 kV.
Quartz	- Easy to obtain - Survives ≤7 kV discharges - Does not alter the plasmoid's optical properties	- Introduces silicone-type ions into the plasmoid at > 5 kV, dominating the MS (overpowering almost all Cu^+ ions).
Alumina	- Only infrequently introduces minor amounts of AlO^+ into the plasmoid – observed in MS	- Brittle; cracks at > 5 kV - Melts slightly - Difficult to machine -

Table 2.2 Materials tested as insulating tubes.

An alternative to using an insulating tube is to have the electrode above the surface of the water, reaching downward to within 1-2 mm of the solution [21]. This produces a plasmoid that

is not as well formed, lacking any indication of a toroidal vortex. Also, the plasmoid seemed to avoid the horizontal electrode as it rose.

The Aqueous Solution

The purpose of the aqueous solution appears to be four-fold. First it serves as a robust, non-flammable dielectric barrier, ensuring an air arc doesn't occur between the central electrode and the ring electrode. Second, it is a resistor, determining the current flow from the capacitors. Third it is semi-conducting surface, limiting the current flow through any particular point at the surface of the liquid, and thereby "encouraging" the plasma's streamers to spread out over the surface of the bucket. Fourth, it is a source of molecules for the plasma to ionize, which are seemingly capable of storing energy for long periods of time.

A variety of aqueous solutions were tested including NaCl, NH_4Cl, HCl, $CuSO_4$, and tap water. The identity of the ions present in the aqueous solution only seemed to affect color of the plasmoid.

As an alternative to producing an electrical discharge over an aqueous solution, an attempt was made to replace the aqueous solution with a conductive silicon wafer. This seemed to be a way to study the phenomenon in the absence of water and potentially allow a way for other compounds to be introduced into the plasma, e.g. for analysis via mass spectrometry. Furthermore it had the potential to merge the floating aspects of our experiments with the long lifetimes observed by Paiva et al., producing a longer lived, less buoyant plasmoid – more similar to what's observed in ball lightning [22]. To test this, a horizontal copper electrode was placed 1 mm above the surface of a silicon wafer which was bonded with silver-epoxy to a copper mesh covering the under-surface of the wafer. The copper and epoxy were encapsulated inside a plastic casing to prevent arcing around the silicon piece. Unfortunately, when the

discharge occurred the silicon shattered, presumably due to the rapid thermal expansion of the wafer caused by resistive heating ($\Delta T > 3000$ K in 50 ms). Further attempts were not pursued, although the same experiment with a ballast resistor following the silicon wafer may be feasible.

2.2 Physical Dimensions Varied

Central Electrode Diameter (d_{CE})

The diameter of the central electrode was tested at 6 mm and 10 mm, resulting in nearly a 3-fold increase in surface area. No differences were observed between the plasmoids produced by the two electrodes, presumably because, in an electrical discharge, the current tends to emanate from a single point on a conductive surface. This was evidenced by "pock marks" on the surface of clean electrodes after several trials.

In order to test the impact of the central electrode's surface geometry on the plasmoid, a "sharp" stainless steel electrode with a pointed cone on top (3 mm tall, 2 mm bottom diameter) was tested. The tip of the cone was 2 mm under water. The resulting plasmoid was much more turbulent, never forming a ball and dying quickly, while a large number of sparks flew from the tip as it was being destroyed. The remaining portion of the tip had a diameter of 2 mm, indicating that this might be the minimal d_{CE} for a stainless steel electrode and that excessive roughness of the electrode might not be favorable.

Central Electrode Depth (h_{CE})

The depth of the electrode below the top of the insulator had a clear impact on the formation of the plasma. As the depth was varied from -5 to 15 mm (increasing the volume of the drop in order to keep the top of the "drop" level with the surface of the quartz), the ball's average upward velocity increased from 72 to 260 cm/s (Figure 2.3). In these trials, a negative

depth means that the copper electrode was above the surface of the quartz insulation. These faster plasmoids prevented much of the plasma from reaching and effectively filling the "ball", producing a narrow, 40% shorter-lived jet of plasma between the electrode and the quickly rising plasmoid (Figure 2.4).

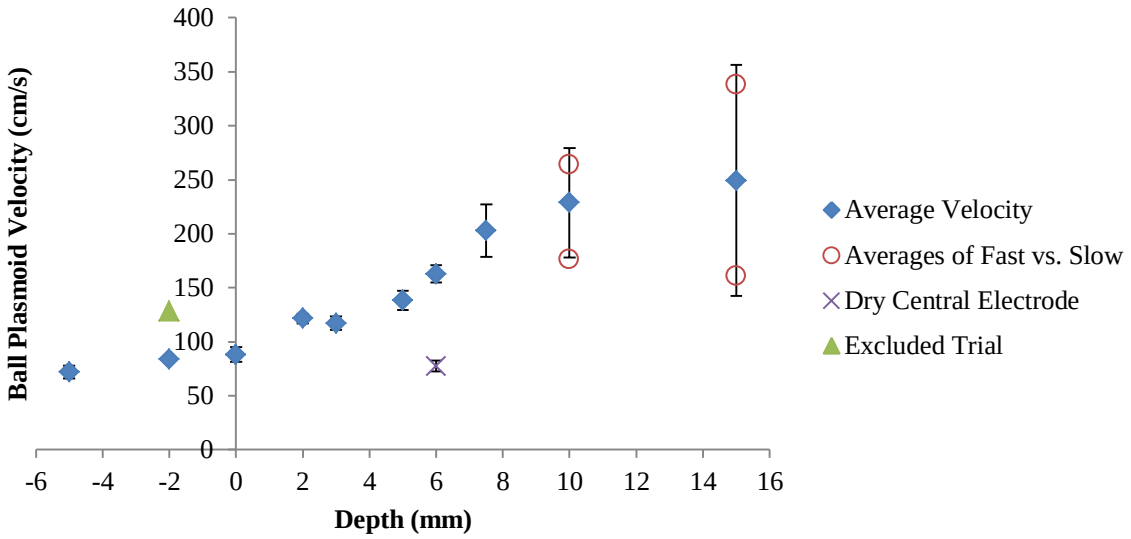

Figure 2.3 The average upward velocity of the ball at various electrode depths. A depth of 0 mm indicates that the electrode was level with the insulation, and a depth of -5 mm indicates that the electrode is 5 mm above the surface of the insulation. The red circles at 10 and 15 cm are the average values of the plasmoid for fast balls and the slow balls as described in the text. Error bars are the standard deviation. The purple "X" is a set of trials in which no water was placed on the electrode but metal was sputtered on the inner surface of the insulating tube as described in Section 2.3.

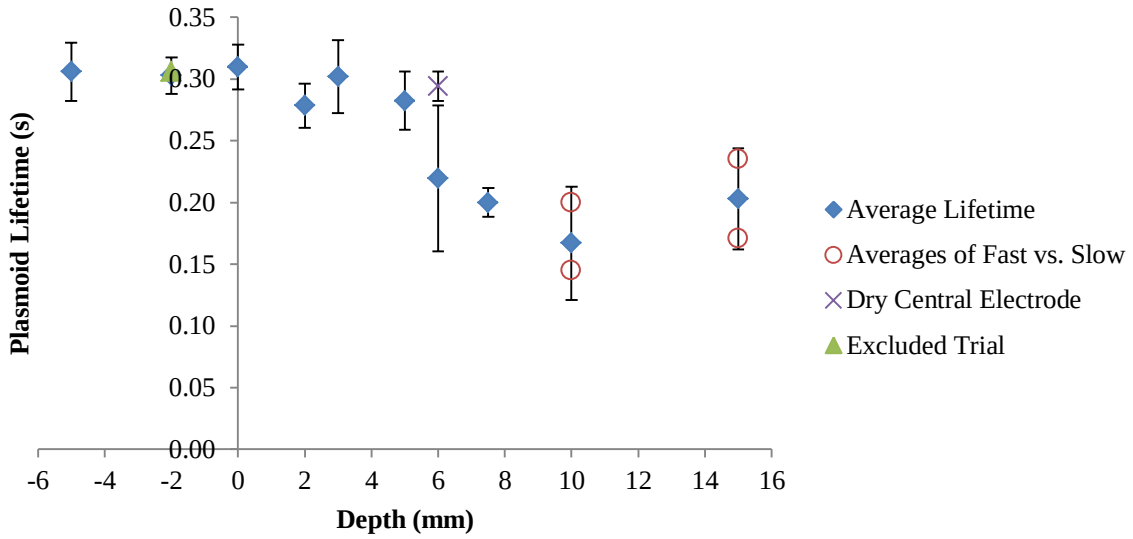

Figure 2.4 The average lifetime of the ball plasmoid for several electrode depths. The red circles correspond to the lifetimes of the fast and slow balls at 10 and 15 cm; the slow balls produced a longer-living plasma. Error bars are the standard deviation.

Several interesting patterns were observed as the depth increased. First, at depths of 10 and 15 mm, the trials fell into two distinct classes, based on their average velocities, designated as fast balls and slow balls. The conditions under which each type plasmoid formed were identical as far as could be controlled. Secondly, it was observed that several of the trials at 10 and 15 mm were "delayed discharges", meaning that there was a delay between when the "Fire" relay closed, connecting the capacitors to the ring electrode, and when the discharge began. Furthermore, a longer delay roughly correlated to a slower and longer lived ball (Figure 2.5). This "delay" might be a lengthening of the pre-initiation phase as described by Stephan et al. [8] in which electrolysis occurs until the current density reaches a few A/cm^2 followed by a brief glow discharge and finally a dielectric breakdown. A further explanation might be that in delayed discharges, the arc is being initiated from the surface of the drop, as opposed to the surface of central electrode.

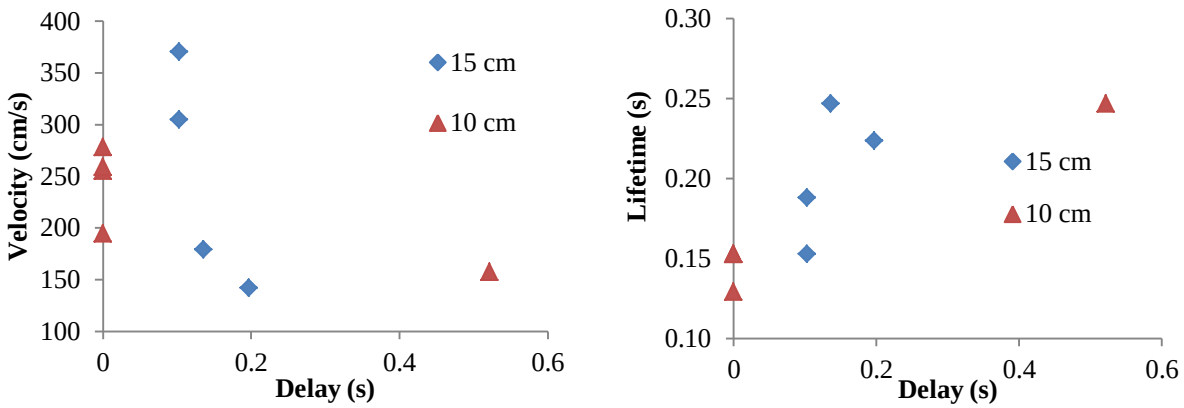

Figure 2.5 a) The velocity and b) lifetime of individual plasmoids produced by electrodes at depths of 10 and 15 cm as a function of the delay before the discharge occurred.

Volume of Water on the Central Electrode, "the Drop" (v_{drop})

The volume of the drop on the central electrode is not a completely independent variable since it must be less than the volume inside the insulating tubing above the central electrode with ~60 µL from surface tension, i.e. a maximum $v_{drop} = A_{CE} \cdot h_{CE} + 60\,\mu L$. Furthermore, it also must the make air-gap length between the drop and the aqueous solution less than that which allows dielectric breakdown (normally < 6 mm total). Therefore, under normal conditions, the volume of the drop is restricted to a range of ~100 µL for d_{CE} = 6 mm. This range was tested with h_{CE} = 2 mm, giving a range of v_{drop} of 0-125 µL, and the plasmoid did tend to have a slightly longer lifetime, as shown in Figure 2.6.

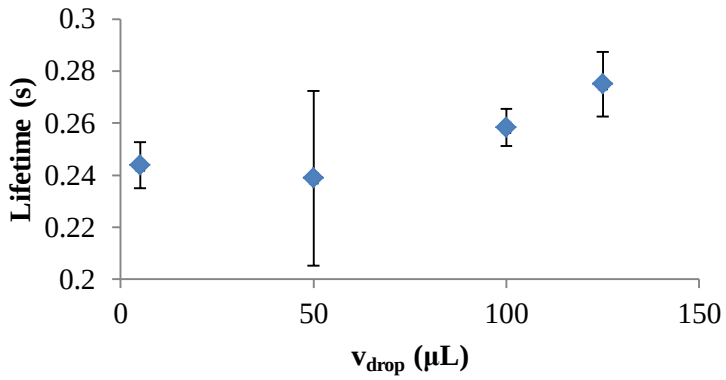

Figure 2.6 The average lifetime of a plasmoid as v_{drop} increases. All discharges were from a 5 kV, 873 µF capacitor over a 280 µS solution. Error bars are the standard deviation.

These results indicate that increasing the amount of water available to be evaporated and ionized early on in the discharge might improve a plasma lifetime. However, a substantial portion of the water is blown off the central electrode due to the rapid thermal expansion of the plasma and is not evaporated. This might be overcome by dropping a thin stream of water onto the electrode, but this was not tested. See Chapter 3.5 for a brief discussion of what happens when a stream of water interacts with a plasmoid itself.

It should be noted that a discharge could occur at larger depths with no drop if the insulating tube was inhomogeneously coated with a thin layer of metal. This was accomplished by slowly increasing the depth of the central electrode (h_{CE}) from 2-6 mm over the series of several trials in which v_{drop} was held at 0 µL. This allowed the copper central electrode to lightly coat the quartz insulating tube with copper via sputtering, allowing several plasmoid-producing discharges at h_{CE} = 6 mm and v_{drop} = 0 µL. However, these plasmoids had very different velocities and different lifetimes than those produced with a drop covering the electrode as shown in Figures 2.3 and 2.4. This indicates that using a deep, dry central electrode with metal sputtered on the insulating tube can be thought of as having an effective electrode depth that is

less than the true electrode depth. Also Figure 2.3 reveals that the increased velocity of the plasmoid at large h_{CE} is in part due to the presence of the water, not just the geometry of the central electrode.

Ring Electrode Diameter (d_{RE}) and Ring Electrode Depth (h_{RE})

Neither the diameter nor the depth of the ring electrode appeared to have a large effect on the plasmoid, aside from what can be attributed to a change in the effective resistance of the aqueous solution (since resistance is dependent on both the length (l) and the area (A) of the resisting material (σ): $R = {}^{l}/_{A\sigma}$). See Section 2.3 – *Conductivity of the Aqueous Solution (σ_{water})* for a further analysis of this point. However, it should be noted that since the aqueous solution is serving as a robust dielectric barrier, it is important that the depth (h_{RE}) not be too small. Otherwise, a high current arc can form between the two electrodes, having a resistance of nearly 0 Ω and producing a loud bang. From experience, arcs can occur at a depth of 3 cm for a 5 kV discharge, but a depth of 6 cm was adequate to prevent arcing, as was discovered while testing Bowl A (described below).

Water Container Size

In an effort to minimize the volume of the water container so that D_2O could be used, two miniature bowls were printed on an AirWolf 3D XL printer. The first of these "bowls" (Bowl A) had the same central electrode as described above, and a d_{RE} = 5 cm, h_{RE} = 3 cm, and a bowl diameter of 15 cm. However, since the depth of the ring electrode (h_{RE}) was too shallow, the plasma arced through the water, producing a very loud bang and throwing all the water out of the bowl. Therefore, a second bowl (Bowl B – Figure 2.7) was made with a d_{RE} = 4.5 cm, h_{RE} = 6 cm, and a bowl diameter of 12 cm, resulting in a total volume of < 200 mL.

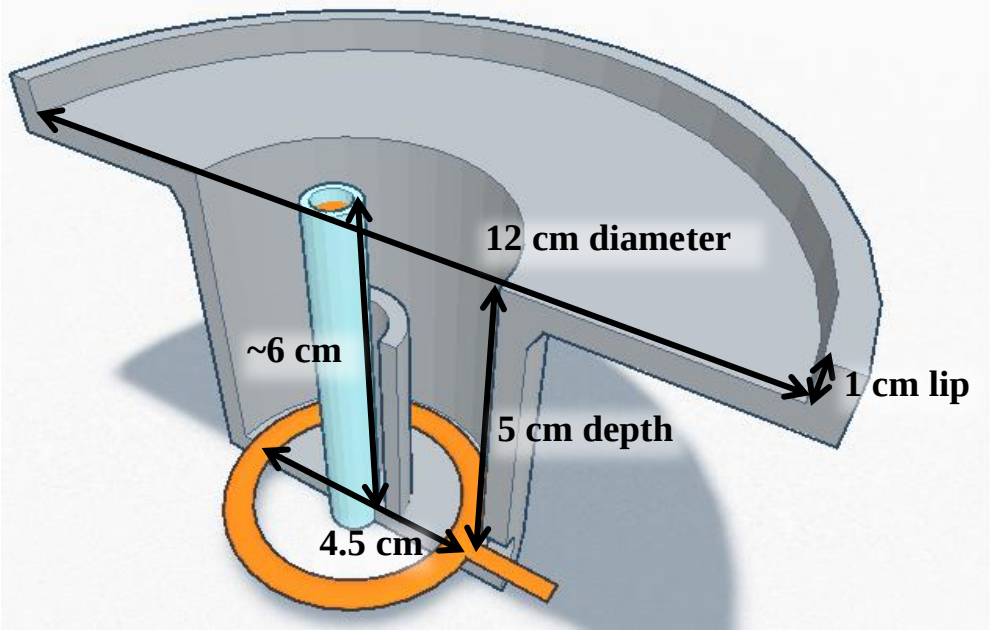

Figure 2.7 “Bowl B”

Based off of the plasmoids produced by Bowl B, the size of the water container containing the two electrodes was found to be unimportant for the formation of the plasmoid. However, if it is important to not introduce impurities into the plasma, then the surface diameter of the container should be > 6 cm larger than the diameter of the ring electrode, otherwise the plasma’s streamers may char the container, introducing impurities into the plasma. Also, when the container’s volume is small, the water can be rapidly heated through resistive heating, changing the resistivity of the aqueous solution.

2.3 Electrical Properties Varied

Polarity of the Plasmoid Generator

As discussed elsewhere [10], the polarity of plasmoid generator is very important for the formation of the plasmoid. When the polarity was reversed, the plasmoid tended to rise at

roughly 60% the speed of a normal plasmoid, but contrary to the normal trend (see Figures 2.3 and 2.4), this slower velocity decreased the lifetime by roughly the same amount.

Conductivity of the Aqueous Solution (σ_{water})

One of the most important parameters involved in generating a well formed plasmoid is the conductivity of the aqueous solution. This was well studied in Friday et al., however, the range of conductivities tested (91-770 μS/cm) did not seem to be wide enough to understand how very high and very low conductivities would affect the formation of the plasmoid. Therefore, a series of similar trials were tested at 1500 and 43 μS/cm, as shown in Figure 2.8. Note that at large conductivities, high energy trials were not tested because of fear of damaging the equipment since the current was > 200 A for a 5 kV, 270 μF discharge over a 1500 μS/cm solution.

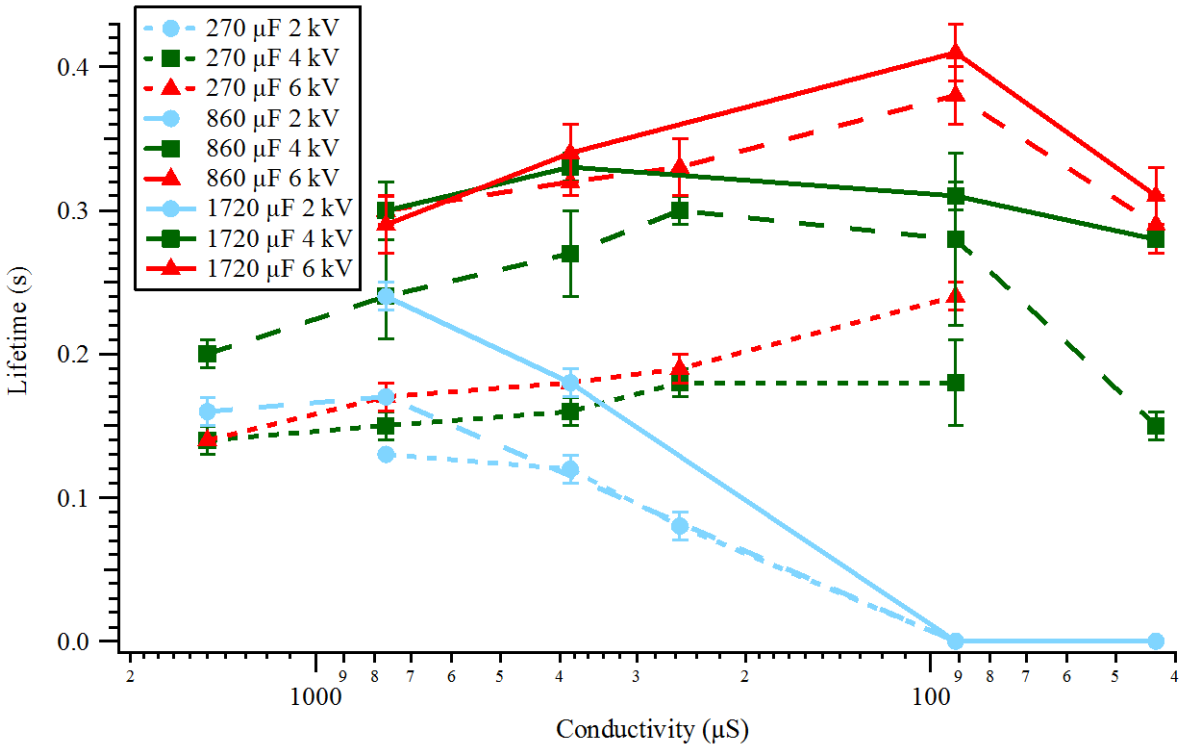

Figure 2.8 The lifetime of the ball plasmoid as a function of conductivity. All data except for conductivities of 43 and 1500 µS/cm were previously published in Friday et al. Note that the conductivity is plotted on a reverselog scale.

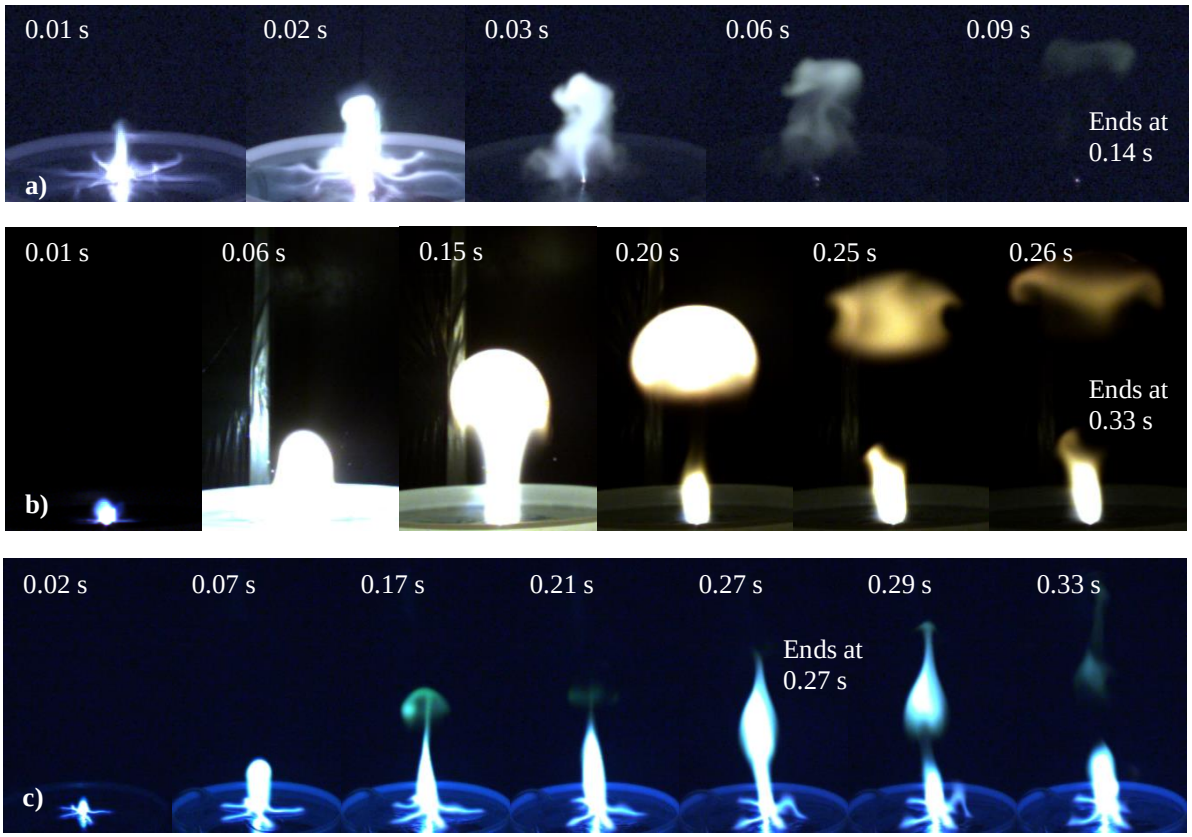

Figure 2.9 A series of frames of a ball produced by a 6 kV, 873 μF discharge over solutions of A) 1500 μS, B) 180 μS, and C) 43 μS. Note that the time scales for each series of images is different and the aperture and distance of the camera were optimized for the size a brightness of the plasmoids. The relative sensitivity of each set of images is 1:2:8 for A:B:C respectively.

This clearly shows that the range previously tested is truly the "sweet spot" for producing well-formed, long living plasmoids. If the solution is too conductive (1500 μS or 3-12 Ω as measured by $R = \frac{V}{I}$), the plasma will expand explosively. This makes the flow very turbulent, preventing it from collecting into a ball structure and dying quickly (see Figure 2.9 a). If the solution is too resistive (43 μS or 1000 Ω), a small ball will form, but the discharge will not produce enough plasma fast enough in order to fill it, causing the weak plasmoid to die quickly as it rises. After this initial plasmoid dies, the continued discharge will produce a flame-like plasmoid above the electrode, followed by an indistinct "flame" as long as the discharge continues (see Figure 2.9 c). As can be seen in frames 0.27-.33 s of Figure 2.9 c) the flame-like

plasmoid following the initial ball does not collect into a ball shape, but is elongated until it dies. It is unclear from the video what causes the plasma to sometimes "pinch-off" successive plasmoids from the electrode or why the second plasmoid fails to form a ball structure. The latter issue is likely explained by an upward flow established by the first ball, preventing the ball from being confined by a body of colder air.

Conductivity of the Drop (σ_{drop})

The conductivity of the drop of the aqueous solution on the central electrode has no significant effect on the formation of the plasmoid, except when the total resistance of the drop $R_{drop} = \frac{h_{CE}}{\sigma_{drop} \cdot A_{CE}}$ is greater than 2 kΩ. If R_{drop} was greater than 2 kΩ, then the likelihood of a delayed ball occurring became greater. However, this was not a perfect trend since a delayed ball occurred at R_{drop} = 1.4 kΩ, but only 1 of 5 plasmoids were delayed at R_{drop} = 3.0 kΩ (given the same h_{CE} and d_{CE}). This variability might be due to metal sputtering up and depositing on the inner surface of the insulation tube, effectively reducing the resistance between the central electrode and the top of the drop.

Voltage and Capacitance

The effect voltage and capacitance has on the plasmoid has been explored in multiple publications [7] [9] [14]. However, due to capacitor limitations, no group has ever tested voltages higher than 6 kV. Therefore, since the equipment used in this research is capable of reaching 10 kV, these higher voltages were tested. However, there was no noticeable gain in plasmoid lifetime between 6 – 10 kV, despite the total energy stored being a function of the square of the velocity ($E = ½ \cdot C \cdot V^2$). This shows that producing long-living, well formed plasmoids is more complicated than simply "dumping" more energy into the discharge.

CHAPTER 3: THE PLASMOID'S ENVIRONMENT

In many publications about ball plasmoids, the authors often mention that the plasmoids were produced in humid environments [1] [10] [23] and some even make claims about the impact the air's humidity and temperature have on the plasmoid [13]. Similarly, several theories attempting to explain the long lifetimes of these plasmoids have small water clusters in the plasma playing a key role in the formation and sustainment of the plasmoid [24] [25]. If this is the case, one might guess that the ambient humidity might affect the plasmoid's lifetime. However, as far as the author is aware, no systematic testing has been reported to show what effect the ambient temperature or humidity have on the plasmoid. Therefore, a series of plasmoids were produced inside an enclosure with specific temperatures and humidities in order to determine the dependence of plasmoid lifetime and velocity on the air's humidity and temperature. Furthermore, a few experiments testing the effect of a laser beam and a stream of water passing through the plasmoid were also tested.

3.1 Experimental Setup

The enclosure used to test the effect of atmospheric temperature and humidity on the plasmoid was a 2'x2'x4' frame with a double layer of black plastic sheets on top and sealing off 3 of the vertical surfaces. A thin sheet of Plexiglas covered the front vertical surface, and black flock paper covered the inside of the rear surface to minimize the reflections of the plasmoid's emitted light off the enclosure's rear surface in the video. The enclosure was not air tight, but it did insulate well enough to let the humidity and temperature inside the enclosure equilibrate while plasmoids were being generated. The enclosure was heated using a heat gun and the humidity was increased by boiling DI water over a hot plate. The humidity and temperature of

every trial was measured with an AM2302 temperature-humidity sensor (±2-5% for 0-100% relative humidity (RH), ±0.5°C for -40-80°C).

3.2 Consecutive Trials

In order to ensure that successive trials in the enclosure would not affect the lifetime or velocity of a plasmoid, a series of 30 plasmoids was produced inside the enclosure as rapidly as possible with a delay of approximately 2 minutes between plasmoids. Over the course of these 30 trials the temperature of the enclosure increased from 21.7°C to 23.3°C and humidity increased from 9.4 to 18.3 g/m^3 (49% to 87% RH). As shown in figure 3.1, neither the lifetime of the trials nor their average velocity showed any substantial changes; both slopes are between one and two standard deviations from having no slope. This ensured that any observed changes in the plasmoid in future trials were truly caused by changes in air's temperature and humidity, not an artifact of simply repeatedly producing plasmoids in an enclosed volume.

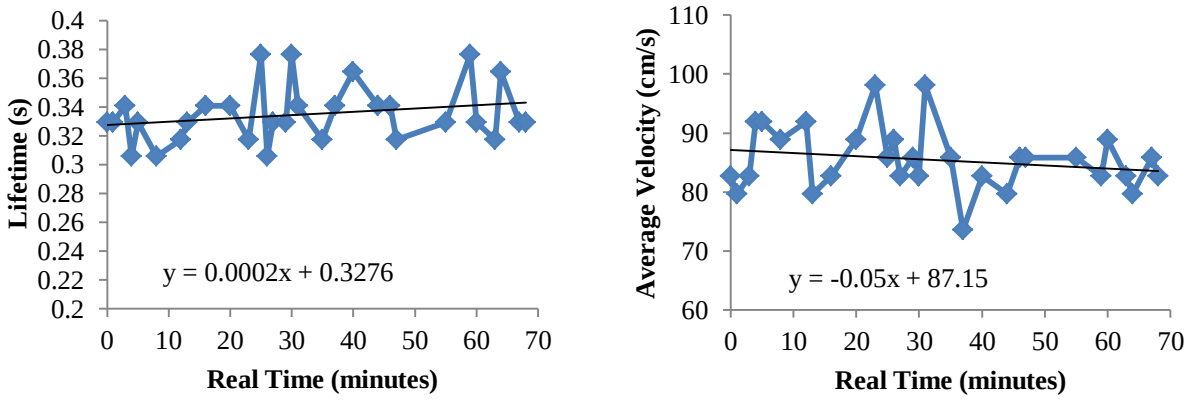

Figure 3.1 The lifetime (a) and average velocity (b) of a series of 30 plasmoids produced over the course of 68 minutes. All plasmoids were produced with 5 kV, 873 µF discharges over a 250 µS solution.

3.3 Temperature

The effect of the ambient air temperature on the plasmoids' lifetime and velocity was tested at 22°C and 39°C (Fig 3.2). The humidity of the ambient air was kept as close to constant as possible; however, due to the increased rate of evaporation at high temperatures, the absolute humidity of the air increased from 12 g/m^3 (62% RH) to 20 g/m^3 (42% RH) between 22°C and 39°C. As seen from these graphs, the average lifetime and velocity are slightly lower at higher temperatures; however, these differences are not statistically significant. Over this range of temperatures the viscosity of the air would have increased by 3%. Therefore, no conclusions about the effect viscosity has on the plasmoid could be drawn from this data, due to the size of the samples' standard deviations.

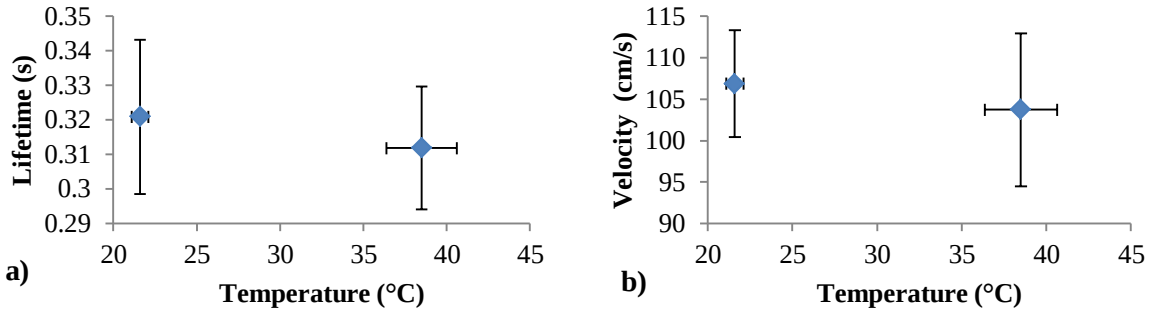

Figure 3.2 a) The lifetime and b) the average velocity of the plasmoids at 21°C and 39°C. The error bars represent a standard deviation. 25 trials were taken at 21°C and 5 trials were taken at 39°C.

3.4 Humidity

The effect of ambient humidity on the lifetime and velocity of the plasmoid was tested over two different aqueous solutions at 40±1.5°C (Figure 3.3). At this temperature, 100% relative humidity is at 52 g/m^3. At a conductivity of 180 µS, 5 trials were taken at 20 g/m^3 (42% RH), and 3 trials were taken at 48 g/m^3 (90% RH). At a conductivity of 300 µS, 4 trials were taken at 8 g/m^3 (15% RH), 8 trials were taken at 48 g/m^3 (89% RH), and then 4 more trials were

taken at 13 g/m^3 (25% RH). As can be seen from Figure 3.3 the absolute humidity of the ambient air did not produce a statistical difference in the lifetime or average velocity of the plasmoids.

This finding does not negate the potential importance of water in sustaining the lifetime of the plasmoid. However, it does indicate that the mixing of ambient moisture into the plasmoid and the role of atmospheric water at the boundary layer of the plasma do not significantly affect the lifetime or velocity of the plasmoid.

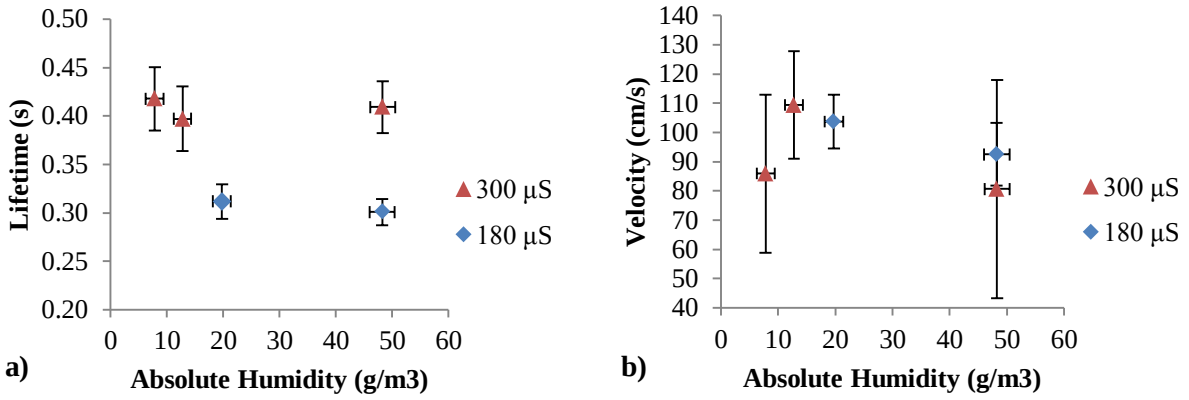

Figure 3.3 The lifetime (a) and average velocity (b) of plasmoids produced from a 5 kV, 860 µF discharge in 40±1.5°C air.

3.5 Miscellaneous Tests

Fog

In order to see if humidities greater that 100% RH alter the plasmoid, several plasmoids were produced with a blanket of fog covering the surface of the aqueous solution produced by an ultrasonic water fogger. The focus of the videos was on the propagation of the initial streamers, which were not different from those of normal trials. However, the plots of current and voltage revealed that having a layer of fog increased the discharge's minimum resistance from 202 Ω to 231 Ω. The cause of this increased resistance is unclear, but it may be due to the additional heating required to turn these additional drops of water into plasma, thereby confining the initial

streamers because the amount of energy required to lengthen a streamer (i.e. ionize the air and water) increases. Therefore, using a fogger could prove to be useful in introducing more water into the plasmoid; however, the conductivity of the aqueous solution would need to be increased to compensate for the added resistance.

Stream of Water Through the Plasmoid

In an effort to introduce water into the interior of the plasmoid, a thin stream of water was forced out of a pipette a slightly downward angle directly above the central electrode. The appearance of the plasmoids was changed in that the stream of water seemed to "trap" a small portion of plasmoid beneath it as seen in Figure 3.4. This could be due to the stream acting like a small barrier, and because the water is cooling a small portion of the plasmoid, decreasing its buoyancy. In contrast to this small portion of trapped plasma, neither the shape nor luminosity of the far (left) side of the plasmoid seemed to be affected by the stream of water.

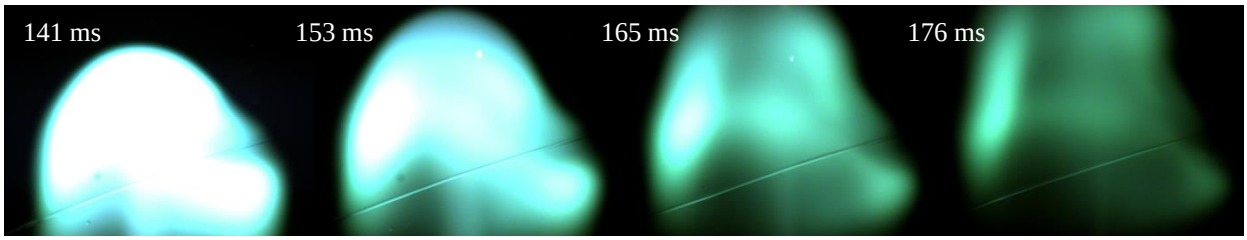

Figure 3.4 A plasmoid rising through a stream of water passing from right to left over the central electrode. As can be seen, a portion of the plasmoid is trapped under the stream of water on the right hand side of the plasmoid.

Lasers

It was reported by [12] that sending a 1 mW red laser (1-10 mW/cm^2, 630-680 nm) through the plasmoid produces a bulge of plasma that grows towards the laser's source. Attempts to reproduce these results were made with a 3.5 mW green laser pointer (532 nm, 20 mW/cm^2), a 20 mW green laser (532 nm, ~150 mW/cm^2), and a 0.5 mW HeNe laser (632nm, 5 mW/cm^2), but none of the videos of these plasmoids showed any altered appearance.

CHAPTER 4: MASS SPECTROMETRY

The most surprising thing about the plasmoids produced in these experiments is their long lifetime. As described in Chapter 1, from recombination rates, one would expect the charges in these plasmoids to have recombined within a few ms after separating from the electrode. However, as is apparent from the videos, light is produced for over 200 ms after separating from the central electrode. Therefore, it seems some unanticipated process is sustaining the emission of the light from these plasmoids. While several theories claim to explain this phenomenon, current data describing the species in the plasmoid is limited to UV-Vis emission spectroscopy, described in Versteegh's master's thesis [26]. Therefore, in an attempt to identify which ions are present in the plasmoid, open air mass spectrometry of the plasmoid was performed.

4.1 Experiment Setup

The mass spectrometer used in this study was a Thermo Scientific LTQ-Orbitrap XL with a 30 cm long stainless steel capillary inlet with a 0.8 mm inner diameter held at ±35 V. The ion trap had a mass detection range of 15-200^{+} m/z, which could resolve peaks at an integer m/z spacing, and was operated at 10^{-5} torr. The orbitrap had a mass detection range of 50-2000 m/z with a precision of < 5 ppm, and was operated at $< 8\times10^{-10}$ Torr [27]. The maximum time resolution was 60 ms/scan for the ion trap and 600 ms/scan for the orbitrap. Depending on the height of the capillary above the electrode, the capillary might be sampling the plasmoid for up to 75 ms, followed by up to 300 ms of flame-like plasma if the resistance was too great (similar to Figure 2.9). Therefore, the ion trap is capable of separating the mass spectrum of the plasmoid from that of the flame-like plasma, but the orbitrap is not.

All plasmoids were produced with the same equipment as described in Chapter 2 with either the 5-gallon bucket or "Bowl B". The central electrode was either copper or tungsten. Copper ions were present in the plasma, facilitating the identification of some small neutral molecules from clustered ions. In contrast, tungsten was never observed in the spectrum. The insulating tube was initially made of quartz until it was realized that silicone-type ions were dominating the spectrum; therefore, all data reported here are from plasmoids produced with an alumina insulating tube. The aqueous solution was always an HCl solution in either H_2O or D_2O with a typical conductivity of 330 μS, although, in Bowl B, the conductivity could range from 190-360 μS. The plasmoids were all generated from a 4 kV, 873 μF discharge unless specifically noted otherwise.

In this chapter, a great amount of variability among mass spectra will be readily observed. Sometimes dominant ions in one spectrum are completely absent from a spectrum taken under identical circumstances. This is because, just like no two bolts of lightning follow identical paths, no two discharges are completely identical either. If the majority of the current remains very near the surface of the alumina insulator, one would expect to see a large amount of alumina-type ions in the plasmoid. Similarly, if the current began to arc through the water near the central electrode it could burn some of the plastic or heat shrink tubing, producing organic impurities. Furthermore, each plasmoid has a slightly different flow structure and they are not perfectly homogeneous, so neither the region nor the composition of the plasmoid sampled by the mass spectrometer is identical in every trial. This variability made it difficult to determine what constituted a "typical" result. However, great effort was taken to systematically analyze all applicable data and report it as concisely and thoroughly as possible.

4.2 Ion Identification

Cations in the Orbitrap

The high mass accuracy of the Orbitrap mass spectrometer allows for easy and nearly certain identification of all ions detected. However, the Orbitrap MS only has a mass range of 50-2000 m/z, meaning it is not capable of detecting small ions. The smallest ion detected in the Orbitrap MS was $C_4H_7^+$ (55.055 m/z); however, when using D_2O as the aqueous solution, the ion trap showed large amount of $D(D_2O)_3^+$ and its isotopologues (55-62 m/z), but these ions were not observed at all in the Orbitrap. This could be due to these cluster ions falling apart in the C-trap or the additional ion optics between the ion trap and the Orbitrap. A full list of ions and their typical relative intensities is presented in Tables 4.1-4. All ions with more than one stable isotope were verified by isotopic mass differences and relative intensities; the reported intensity of each ion is the sum of all isotopes. All ions identified had mass accuracy of < 5 ppm, typically < 2 ppm.

When a copper central electrode was used, there were always substantial amounts of copper-based ions as shown in Table 4.1 and Figure 4.1.These types of ions were easily identifiable by the isotopic ratio and the mass difference between copper's two isotopes ^{63}Cu (61%) and ^{65}Cu (39%).

Ion	Average Intensity	%Standard Deviation	Trials Averaged
Cu	17	29%	7
Cu NH_3	27	25%	7
Cu H_2O	133	25%	7
Cu $(NH_3)_2$	4.7	67%	7
Cu NH_3 H_2O	35	24%	7
Cu $(H_2O)_2$	100	---	7
Cu CH_3CN	128	56%	3
Cu H_2O N_2	11	6%	3
Cu CH_3CN H_2O	124	31%	2
Cu NO_3 H_2O	495	9%	2
Cu NO_3 $(H_2O)_2$	268	6%	2
Cu_2 OH NO_3 H_2O	87		1
Cu_2 NO_3 $(H_2O)_2$	53		1
Cu $C_{13}H_{22}O$	24		1
Cu_2 NO_3 CO_2 $(H_2O)_2$	29		1
Cu_2 OH $(NO_3)_2$ H_2O	74		1
Cu_2 $C_2H_6O_7N$	20		1
Cu $C_{12}H_{24}O_6N$	22		1

Table 4.1 A summary of the copper-based ions observed in the plasmoid when using a copper electrode. The intensity of all ions in each spectra were normalized to $Cu(H_2O)_2$ having a standard intensity of 100, and then averaged. All ions have a +1 charge, and any grouping of atoms into molecules is presumed, but not proven.

In an attempt to better observe the plasmoid's mass spectra in the absence of copper ions, a tungsten central electrode was used. However, as is shown in Table 4.2, several silver and lead ions, as well as organic ions (Table 4.4) were in the plasmoid's mass spectrum. The source of the silver and lead based ions is likely the solder used to secure the high voltage wire to the insulated electrical bus which was connected to the central electrode. It should be noted that solder's primary component, tin, was completely absent from the mass spectrum.

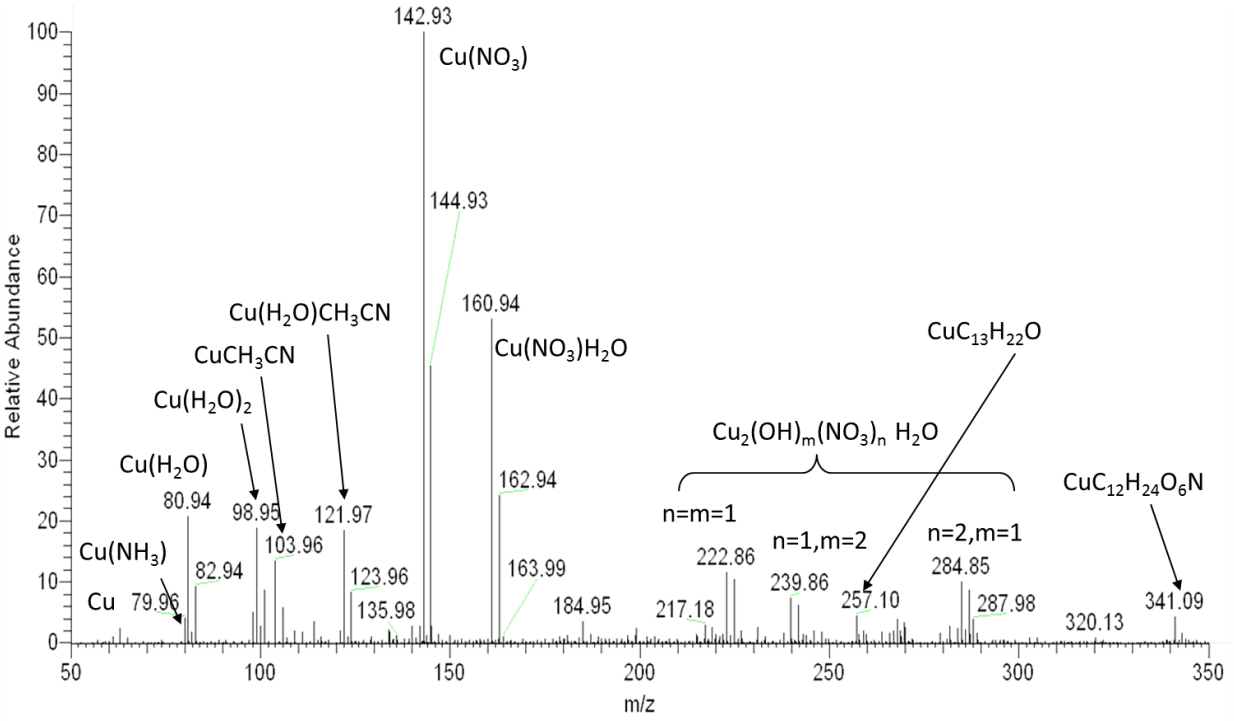

Figure 4.1 A mass spectrum of a plasmoid from a copper electrode.

Ion	Intensity	Ion	Intensity
Ag	12	Pb OH	15
Ag NH_3	14	Pb OH H_2O	13
Ag H_2O	99	Pb Cl	8.2
Ag $(NH_3)_2$	1.7	Pb Cl H_2O	68
Ag $(H_2O)_2$	12	Pb NO_2	13
Ag NH_3 H_2O	2.3	Pb NO_2 H_2O	100
Ag CH_3CN	4.3	Pb NO_3	27
Ag C_3H_6O	3.6	Pb NO_3 H_2O	59
Ag C_3H_7ON	8.6	Pb $C_2H_3O_2$	95
Ag $C_3H_8O_2$	1.2	Pb $C_2H_3O_2$ H_2O	36
Ag $C_3H_9O_2N$	1.8	Pb $C_4H_7O_2$	85
		Pb $C_4H_7O_2$ H_2O	24

Table 4.2 A summary of silver and lead based ions present in a plasmoid produced with a tungsten electrode. All ions were normalized to the most intense ion in the spectrum (Pb NO_2 H_2O) having an intensity of 100. All ions have a +1 charge, and any grouping of atoms into molecules is presumed, but not proven.

In addition to the ions produced by the central electrode, a few plasmoids produced with a copper electrode contained notable amounts of alumina based ions, reported in Table 4.3. The alumina based ions tended to either be very prominent or nearly absent from any given spectrum, being very strong in 3 of 12 spectra covering the m/z range of these ions, and having an intensity of 0-1% of the maximum intensity in the other 9 spectra. This indicates that some unpredictable dielectric breakdown or melting event occurred, producing these ions. All values in Table 4.3 are the average of only the spectra containing these ions.

	Average Intensity	%Standard Deviation	Trials Averaged
AlO H_2O	0.5		3
AlO $(H_2O)_2$	56	20%	4
AlO $(H_2O)_3$	100	---	4
Al $(H_2O)_2$ N_2 NO	48		1
AlO NO_3 OH	8.7		1
Al_2O_2 $(H_2O)_3$ OH	108	2%	2
Al_2O_2 $(H_2O)_2$ OH N_2	48		1

Table 4.3 A summary of alumina based ions present in the plasmoid, showing the average intensity of each ion with each trial individually normalized to $Al(H_2O)_3$ having a standard intensity of 100. All ions are singly charged, and any grouping of atoms into molecules is presumed, but not proven.

As the previous tables have shown, the most common molecule attached to these metal ions is clearly water, which comes from both the bucket of water, humidity, and from within the mass spectrometer (as discussed in section 4.4). The other small clustered molecules are either presumably produced in the plasma or are impurities introduced into the plasma from the surroundings. As will be discussed in section 4.4, when using a D_2O solution, the ratios of hydrogen to deuterium in NH_3 indicate that NH_3 is actively produced in the plasmoid. To the author's knowledge, this is the first detection of NH_3 in an air-water plasma. In contrast, CH_3CN

never contained deuterium, indicating that it is introduced by the bowl since it is commonly found in ABS and completely miscible with water. The remaining molecules (NO_2, NO_3, and OH) and their ions are each commonly observed in air plasmas [28]. It should be noted that these observed intensities are not proportional to the actual concentration of these molecules in the plasmoid since the binding energy of each of these molecules is different.

The last large group of ions observed via orbitrap is the organic based ions, shown in Table 4.4. These ions presumably originated from impurities in the experiment – human oils, burned electrical tape or plastic, dust in the air, etc. The total intensity of all these ions was typically less than 10% of the intensity of the copper-based ions. However, in the first spectrum acquired after replacing the central electrode, the sum of the intensities of the organic ions was 75% that of the copper-based ions. Therefore, care must be taken to ensure the plasmoid generator is free of any oils if one requires a clean spectrum, but producing a few plasmoids does effectively clean the plasmoid generator. Table 4.4 also shows the ions produced using a tungsten electrode, which had more higher-mass impurities. For the sake of comparison, the intensity of the most intense organic ion (C_3H_8ON) is 89% the intensity of Pb H_2O NO_2 in Table 4.3.

As can be seen in Table 4.4, a wide variety of organic ions were observed, however a few trends can be observed in this wealth of data. First, there is a small subset of ions that appear to be the result of an NO^+ attached to a neutral hydrocarbon (C_2H_6, C_3H_8, C_5H_8, C_5H_{10}, C_6H_{12}). Interestingly, none of these hydrocarbons contain an oxygen atom. This indicates that most neutral organic molecules in the plasmoid do not contain oxygen. This is corroborated by the fact the plastic ABS bowl and polyolefin heat shrink contain no oxygen, and that fatty acids in human oil contain miniscule amounts of oxygen. Therefore there are no sources of oxygen-containing

hydrocarbons. However, most of the ionic hydrocarbons not containing NO^+ contain 1 or 2 oxygen atoms, many of which cannot be explained by simply adding a water to an existing ion (i.e.C_3H_7O, C_4H_7O, C_5H_7O, $C_5H_7O_2$, C_6H_7O, $C_6H_{11}O$, $C_6H_{15}O_3$). Therefore, it appears that these hydrocarbons were oxidized by the plasma, demonstrating the presence of reactive oxygen in the plasmoid, most likely OH.

Ion	"Copper"	"Tungsten"	Ion	"Copper"	"Tungsten"
CH_5ON_2	100	0	$C_6H_{11}O$	10	0
C_2H_6ON	2	0	$C_6H_{12}ON$	0	35
$C_3H_5O_2$	2	0	C_6H_{13}	3	0
C_3H_7O	8	0	$C_6H_{13}O$	7	0
C_3H_8ON	12	100	$C_6H_{15}O_3$	0	14
C_4H_7O	7	0	C_7H_7	2	0
$C_4H_7O_2$	12	0	C_7H_9	5	0
C_4H_9	19	0	C_7H_9O	3	0
$C_4H_9O_2$	14	0	C_7H_{11}	14	0
C_5H_7	5	0	$C_7H_{18}N$	6	0
C_5H_7O	4	0	C_8H_{11}	6	0
$C_5H_7O_2$	12	0	C_8H_{13}	9	0
C_5H_8ON	7	0	C_8H_{15}	0	20
C_5H_9	8	0	$C_8H_{15}O$	0	11
C_5H_9O	15	0	$C_8H_{15}O_2$	0	18
$C_5H_9O_2$	19	10	$C_8H_{17}O$	0	11
$C_5H_{10}ON$	93	60	$C_8H_{19}O_3$	0	47
C_5H_{11}	4	0	$C_{12}H_{23}O_2$	0	35
C_6H_7O	3	0	$C_{12}H_{23}O_3$	0	18
C_6H_{11}	11	0	$C_{12}H_{25}O_3$	0	58

Table 4.4 A summary of organic ions present in the plasmoid. The first column of intensities, “Copper” is the sum of 7 trials with a copper electrode, the large majority of the ions of which were produced by the first plasmoid. The second column of intensities was observed in the plasmoid produced by the tungsten electrode in which silver and lead ions were also observed.

A final small group of ions observed in a few spectra were designated $MnNO_3(H_2O)_n$ (n = 0-2). The only known potential source of manganese is the stainless steel capillary, which seems an unlikely source, making this assignment tentative. However a complete lack of other reasonable ions with an appropriate mass and no observable isotopes forced this assignment. These ions are only important in studying the ratios of hydrogen and deuterium in Section 4.3.

Cations in the Ion Trap

As mentioned above, the ion trap has two major advantages over the orbitrap. First, it is able to detect ions with mass-to-charge ratios less than 50 m/z. Second, it has a high time resolution capable of detecting the ions in the ball-plasmoid separately from the ions in the flame-like plasma. However, due to the ion trap's low spectral resolution it is difficult to identify ions with great certainty unless supported by using MS-MS, isotopic distributions, or a lack of reasonable alternatives. The most common masses and their corresponding ions are presented in Table 4.5. It is clear from the percent standard deviation that the concentrations of these ions in the plasmoids can vary greatly from spectrum to spectrum. These ratios will be discussed further in section 4.4.

When D_2O was used, all ions showed the expected mass shifts as shown in Figure 4.2 and described in detail in Section 4.3. MS-MS was attempted with $H(H_2O)_3^+$ but no substantial amounts of ions were ever observed in the MS-MS spectrum.

m/z	Ion	Ave. Intensity	%Standard Deviation
30	NO^+	34	52%
37	$H(H_2O)_2^+$	69	84%
48	$NO(H_2O)^+$	100	49%
55	$H(H_2O)_3^+$	48	36%

Table 4.5 The most common ions observed in the ion trap with their average intensities in the first 180 ms of scans and the percent standard deviation of those intensities across the 6 trials.

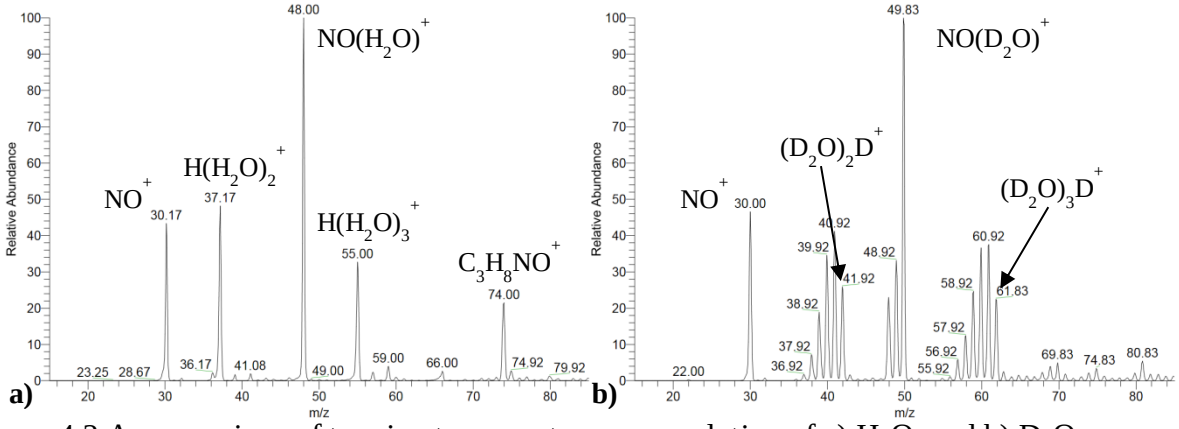

Figure 4.2 A comparison of two ion trap spectra over a solution of a) H_2O, and b) D_2O.

Anions in the Plasmoid

In addition to positively charged ions, 3 negatively charged ions were weakly observed in the Orbitrap, as shown in Table 4.6. Although the presence of negative ions is rare in a plasma, 3-body electron attachment is possible if the gas temperature is low and the electron temperature is less than 0.5 eV (5500K) [29], which agrees with [16]. Using the extended low mass range of the ion trap, an additional small signal was observed at 42 m/z and was assigned to NO_2^-.

Ion	Intensity (Orbitrap)	Intensity (Ion Trap)
NO_2^-	0	4
NO_3^-	100	100
$HN_2O_5^-$	9.2	45
$HN_2O_6^-$	59	7

Table 4.6 A summary of all the negatively charged ions observed in the plasmoid. All ions are singly charged.

4.3 Hydrogen and Deuterium Distributions

In order to confirm the identity of the protonated water clusters in the ion trap's spectra, several plasmoids were generated over a ~99% D_2O – HCl solution in Bowl B. As expected, the ions in the ion trap that were thought to contain hydrogen atoms showed appropriate mass shifts. The presence of deuterium was easily distinguished in the orbitrap by its very unique mass difference of +1.0063 m/z from hydrogen.

However, surprisingly, in most of the water containing ions, the distribution of hydrogen and deuterium within each ion was not a binomial distribution, and a surprisingly large amount of hydrogen was present (15-55%). This strong divergence from the expected binomial distribution prompted a more thorough analysis of the distribution of hydrogen and deuterium in the water-containing ions, providing new data supporting the plasmoid's unique ability to protect its ions from the atmosphere.

Modeling the Distribution of Hydrogen and Deuterium

Before discussing how the isotopic distributions do not indicate a complete randomization of hydrogen and deuterium, here is a brief summary of how to calculate the ratios of isotopologues assuming a random distribution of all isotopes, using the binomial distribution. In general, to find the ratios of the isotopologues of a molecule with *n* atoms being one of two isotopes, one can use the following equation in which *p* is the fractional amount of each isotope,

k is the number of that isotope present in the molecule, and $\binom{n}{k}$ is the appropriate binomial coefficient:

$$\text{Probability}(k) = \binom{n}{k} p^k (1-p)^{n-k}$$

For example, to find the ratios of the isotopologues of $Cu(H_2O)_2$ (n = 4) given the fractional amount of deuterium (p = %D), one would find that:

$$\Pr(CuD_kH_{4-k}O_2) = \binom{4}{k} \%D^k (1-\%D)^{4-k}$$

Surprisingly, this type of pattern was only observed in the ammonia-containing compounds. In order to model these distributions, it was thought that maybe these seemingly complex distributions can be modeled as a randomized mixture of H_2O, HDO, and D_2O molecules starting with arbitrary (non-binomial) distributions of H_2O's isotopologues.

To parameterize an arbitrary distribution of H_2O's isotopologues, two constants were defined: the percent deuterium of all the H_2O isotopologues ($\%D_{raw}$), and the amount of mixing between hydrogen and deuterium (%Mixed). As shown in Figure 4.3, if a distribution is 0% mixed, only H_2O and D_2O will be present, however if a distribution is 100% mixed, the amounts of H_2O, HDO, and D_2O will be a binomial distribution. Intermediate cases are a linear combination of these extremes.

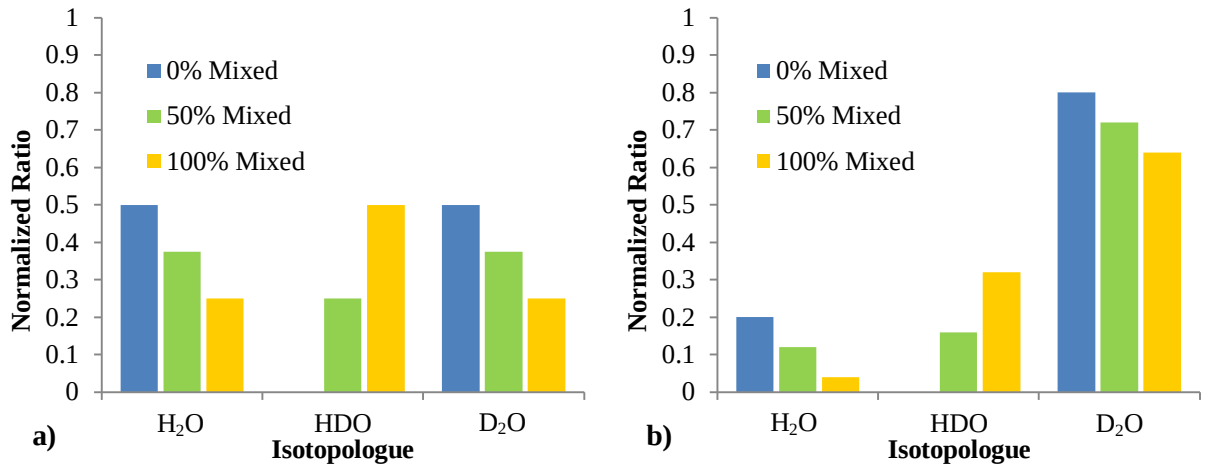

Figure 4.3 An example distributions of H_2O's isotopologues produced using the parameters $\%D_{raw}$ and %Mixed. a) is a distribution given a $50\%D_{raw}$, and b) is a distribution given an $80\%D_{raw}$.

In order to model ions with two or three water molecules, the distribution of H_2O isotopes was convoluted with itself using the following formulas in which brackets indicate a normalized concentration.

$$[H_kD_{4-k}O] = \sum_{n+m=k} [H_nD_{2-n}O][H_mD_{2-m}O] \quad 0 \le n, m \le 2;\ 0 \le k \le 4$$

$$[H_kD_{6-k}O] = \sum_{n+m+l=k} [H_nD_{2-n}O][H_mD_{2-m}O][H_lD_{2-l}O] \quad 0 \le n, m, l \le 2;\ 0 \le k \le 6$$

For example, Figure 4.4 b) shows how a $44.8\%D_{raw}$ and 31.5%Mixed distribution is convoluted with itself to produce the total distribution of all five isotopologues of $Cu(H_2O)_2$. Modeling protonated water clusters was slightly less straight forward since the raw, unhydrated ion could be considered H^+ or H_3O^+, and both of these ions should have their own isotopic distribution. To account for this, the procedure was modified so that the added water molecules were convoluted with isotopic distributions of H^+ or H_3O^+ as determined using the same $\%D_{raw}$ and %Mixed described above except that n = 1 or 3, instead of 2 as in the case of H_2O. Similarly,

if NH_3 was attached to an ion, $n = 3$, and its distribution was calculated and convoluted in the same way.

Using this model, all isotopic ratios were fit to a $\%D_{raw}$ and a %Mixed so that the distribution of hydrogen to deuterium could be consistently compared between ions with different numbers of hydrogen atoms. In the ions containing more than 2 hydrogen atoms, first the $\%D_{raw}$ across all isotopologues was calculated, and then the optimal %Mixed that minimized the squares of the differences between the model and the data was found.

As an example, $Cu(H_2O)_2$ had the isotopic distribution shown in Table 4.7 and Figure 4.4 a). The percent deuterium ($\%D_{raw}$) of this ion was found by summing the products of the isotopes' normalized ratios and the fractional amount of deuterium present.

$$\%D_2O_{raw} = [CuD_4O_2] + \tfrac{3}{4}[CuD_3HO_2] + \tfrac{1}{2}[CuD_2H_2O_2] + \tfrac{1}{4}[CuDH_3O_2]$$

Then the two extreme cases for a distribution, no mixing and perfect mixing (a binomial distribution) were modeled, and linearly combined using an arbitrary mixing ratio. In essence, for H_2O in Table 4.7 d), 0.552·(1-%Mixed) + 0.305·(%Mixed) = Model Ratio. From these ratios of H_2O:HDO:D_2O, the full distribution was calculated by summing the products of each combination of H_2O's isotopologues that resulted in a given number of deuterium atoms.

$$[CuD_2H_2O_2] = [H_2O][D_2O] + [HDO][HDO] + [D_2O][H_2O]$$

This model was then refined by choosing the %Mixed that minimized the sum of the errors between the data and the model, squared.

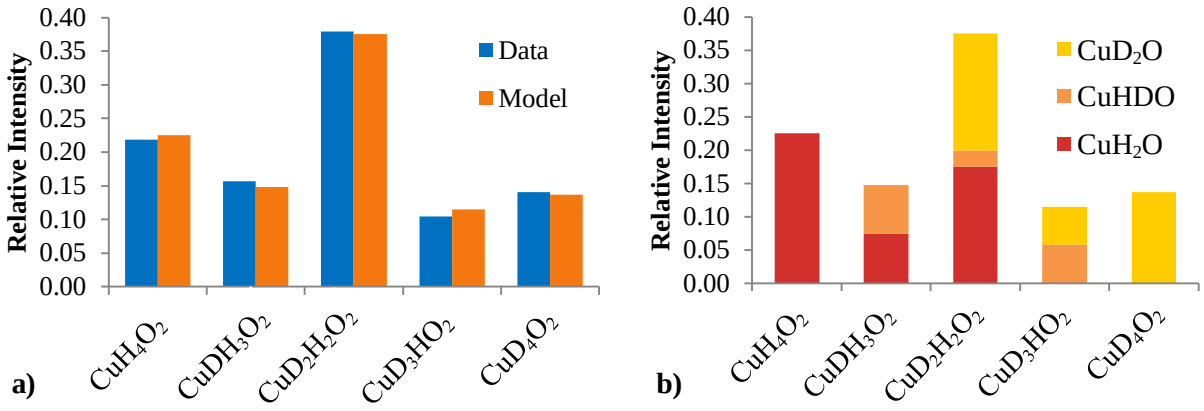

Figure 4.4 a) The distribution of $Cu(H_2O)_2^+$ isotopes in the orbitrap spectrum when using D_2O, and the modeled distribution calculated as described above. b) A breakdown of the model showing the convolution of two water molecules with the same isotopic distribution with each other. These graphs are shown numerically in Table 4.7.

a)

Isotopologue	Ratios
$CuH_4O_2^+$	0.219
$CuDH_3O_2^+$	0.157
$CuD_2H_2O_2^+$	0.379
$CuD_3HO_2^+$	0.104
$CuD_4O_2^+$	0.141

b)

$\%D_{raw}$	44.8%

c)

%Mixed	0.315

d)

	0% Mixed	100% Mixed	Model Ratios
H_2O	0.552	0.305	0.475
HDO		0.495	0.156
D_2O	0.448	0.200	0.370

e)

Isotopologue	Ratios	$(Error)^2$
$CuH_4O_2^+$	0.225	0.0000
$CuDH_3O_2^+$	0.148	0.0001
$CuD_2H_2O_2^+$	0.375	0.0000
$CuD_3HO_2^+$	0.115	0.0001
$CuD_4O_2^+$	0.137	0.0000

Table 4.7 Example isotopic analysis calculations. a) The isotopic distribution to be modeled. b) The calculated percent deuterium $\%D_{raw}$ from (a). c) The mixing ratio %Mixed. d) The predicted ratios of a single water molecule given the $\%D_{raw}$ and %Mixed. e) The modeled isotopic distribution and the square of the differences between the experimental data (a) and the model.

Validating and Applying the Model to the Data

This model proved to be very effective in reducing a distribution of several isotopologues to two parameters that had an intuitive explanation. However, in order to ensure that the model accurately fit each distribution with more than 2 hydrogen atoms, criteria had to be made to determine when the model fit the data accurately enough to consider the distribution of H_2O:HDO:D_2O a valid simplification of the more complex distribution.

In the case of the orbitrap spectra, the ratios of each isotopologues could be precisely determined since the orbitrap had a high resolution and mass accuracy. Therefore, the sum of the squares of the differences between the data and the model had to be less than 0.002 in order for the model to be considered valid, as was always the case.

The distribution of isotopes in the ion trap's mass spectra required a more complicated analysis since two ions with the same integer mass could not be resolved (i.e. $H_3D_2O_2^+$ and $^{39}K^+$). Therefore more specialized criteria were applied for the 4 ions studied in the ion trap: $H_5O_2^+$, $H_7O_3^+$, $NO(H_2O)^+$, and $Cu(CH_3CN)(H_2O)^+$. However, regardless of modifications, all models for ion trap data needed to have a sum of squares error (SSE) less than 0.01.

For the protonated water clusters ($H_5O_2^+$ and $H_7O_3^+$), $^{39}K^+$ ions were occasionally observed in ion trap spectra and have the same integer mass as $H_3D_2O_2^+$. Similarly, $^{39}K(H_2O)^+$ ions have the same integer mass as $H_5D_2O_3^+$. Therefore, if there was a notable excess of mass 39 m/z or mass 57 m/z in the data, the model was optimized for the ratios of the other 4 or 6 isotopes.

For $NO(H_2O)^+$, no notable impurities were typically present in the mass ranges of its isotopologues. Also, since there are only three isotopologues, no further validation could be made.

For copper based ions, the purity of each ion's signal in the mass spectrum could be relatively easy to assess since ^{63}Cu and ^{65}Cu have a ratio of 1:0.45, making it possible to determine if other unresolved ions were present. After a brief look, it was found the at $Cu(H_2O)^+$ and $Cu(H_2O)_2^+$ were not suitable options, but that $Cu(CH_3CN)(H_2O)^+$ was. Two criteria were used to determine the validity of a spectrum. First, the ratio of $^{63}Cu(CH_3CN)(HDO)^+$ to $^{65}Cu(CH_3CN)(HDO)^+$ had to be between 0.31 and 0.58 (30% from the known ratio 0.45).

Second, since $^{63}Cu(CH_3CN)(D_2O)^+$ and $^{65}Cu(CH_3CN)(H_2O)^+$ could not be resolved (124 m/z), the sum of the predicted amount of $^{63}Cu(CH_3CN)(D_2O)^+$ (as determined by dividing the intensity of the $^{65}Cu(CH_3CN)(D_2O)^+$ by 0.45) and the predicted amount of $^{65}Cu(CH_3CN)(H_2O)^+$ (as determined by multiplying the intensity of the $^{63}Cu(CH_3CN)(H_2O)^+$ by 0.45) had to be less than 30% different from the observed intensity of the 124 m/z peak. If both these criteria were met, then the sum of squares error was always less than 0.01.

As a visual aid, Figure 4.5 shows several isotopic distributions with different sum of squares error (SSE). The data shown in Figure 4.5 is the strongest signal observed for $H_7O_3^+$ and it showed very good agreement with the optimal model produced using the procedures described above (SSE = 0.00005, 56%Mixed). To show what a typical error looks like, the model was intentionally given a sub-optimal %Mixed (42% vs. 56%) that had the average SSE for all the data considered in the following analysis (average SSE = 0.0017), and this distribution was graphed as the "Average Model" in Figure 4.5. Lastly a binomial distribution (100%Mixed) of hydrogen and deuterium was graphed, which would have been considered an invalid model (SSE = 0.0104).

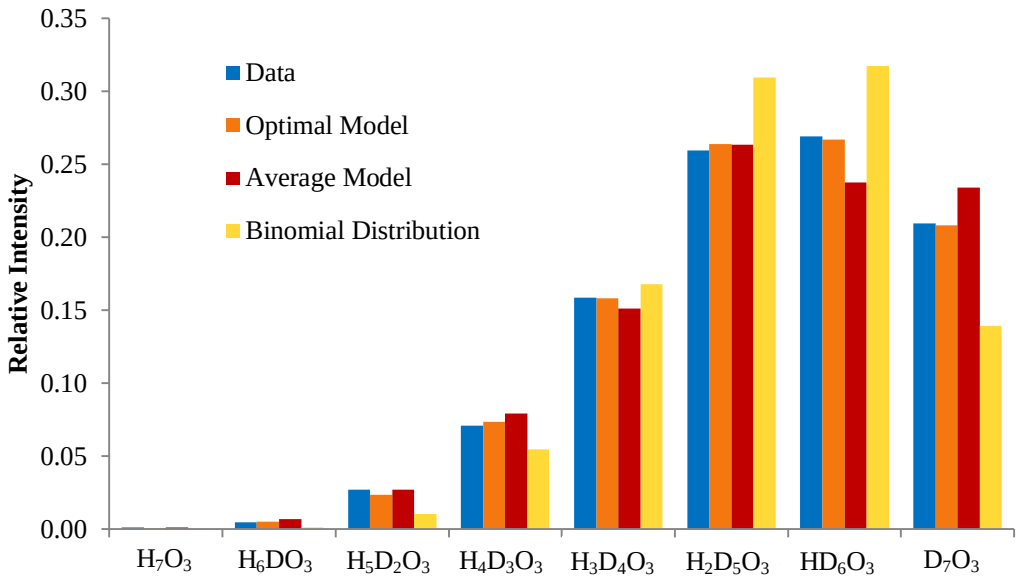

Figure 4.5 A distribution of deuterated $H_7O_3^+$. The optimal model was produced via the procedure described above and had a SSE of 0.00005. The average model was intentionally given a %Mixed that produced a SSE of 0.0017, showing the average amount of deviation of a typical fit. The binomial distribution had a SSE of 0.0103.

Calculating the $\%D_{binomial}$ in the Plasmoid

After the modeled ratios of H_2O:HDO:D_2O for each ion were found, the percent deuterium ($\%D_{binomial}$) could be calculated. The $\%D_{binomial}$ is the percent deuterium that would produce the same ratio of HDO:D_2O in the model if all the deuterium atoms were distributed binomially. Mathematically, this is described by the following equations in which [D_2O] and [HDO] are from the model described above:

$$\frac{[\mathrm{D_2O}]}{[\mathrm{HDO}]} = \frac{(\%D_{binomial})^2}{2(\%D_{binomial})(1-\%D_{binomial})}$$

$$\%D_{binomial} = \frac{2[\mathrm{D_2O}]}{[\mathrm{HDO}]+2[\mathrm{D_2O}]}$$

This new distribution grossly underestimates the amount of H_2O present in a distribution as shown in Figure 4.6; however, it describes the percent deuterium if there were free mixing between H and D atoms in water molecules, followed by a sizable amount of H_2O added after

that period of mixing had ceased. The usefulness and validity of this metric will become apparent when analyzing the isotopic distributions. In this model, if all hydrogen and deuterium atoms were perfectly mixed, then $\%D_{binomial} = \%D_{raw}$, and if they were 0% mixed (i.e. no HDO in the modeled ratios), then $\%D_{binomial} = 100\%$.

Results

Table 4.8 and Figure 4.6 provide a summary of the $\%D_{raw}$ and $\%D_{binomial}$ observed in the orbitrap. In the spectrum, there was a large variety of $\%D_{raw}$ for each ion (42-85%), but a very small variation in the $\%D_{binomial}$ (80-86%). For the NH_3 containing ions, the $\%D_{raw}$ and $\%D_{binomial}$ are practically identical indicating that the ratio of H to D present in the plasmoid as the ammonia was formed was ~85%. Interestingly, all the water based ions have essentially the same $\%D_{binomial}$, although a wide variety of $\%D_{raw}$. This indicates that there is a certain amount of H_2O (19-25% the amount of D_2O) that is introduced and is able to exchange nuclei with the D_2O present in the plasma. Additionally, there is also a variable amount of extra H_2O (50-120% the amount of D_2O) that is introduced into the plasmoid which does not exchange its protons with the existing mixture. The source of this extra H_2O is unclear from this data; however the three most probable sources seem to be the humidity in the air, water adsorbed onto the surface of the capillary, or adsorbed water inside the mass spectrometer.

Species	$\%D_{raw}$	$\%D_{binomial}$
$Cu(H_2O)$	42%	82%
$Cu(CH_3CN)(H_2O)$	43%	85%
$Cu(NO_3)(H_2O)$	40%	82%
$Cu(H_2O)_2$	43%	82%
$Cu(NO_3)(H_2O)_2$	45%	83%
$Mn(NO_3)(H_2O)$	55%	84%
$Mn(NO_3)(H_2O)_2$	60%	84%
$Cu(NH_3)$	82%	85%
$Cu(NH_3)_2$	85%	86%

Table 4.8 Percent deuterium observed for each ion observed in the orbitrap. Note that the assignment of $MnNO_3$ is tentative; however, the mass of the ion clearly indicates it is metal-based and is hydrated twice.

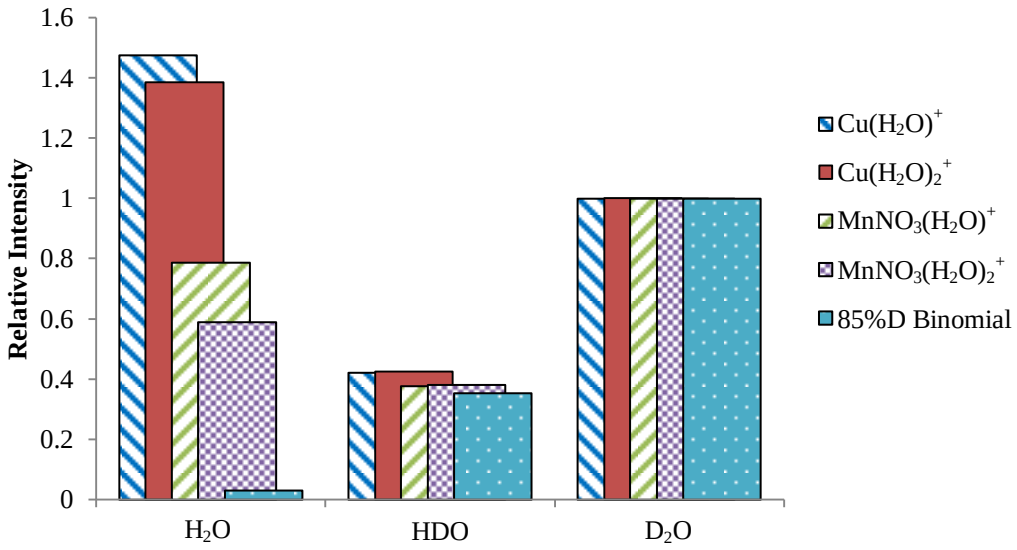

Figure 4.6 The distribution of H_2O, HDO, and D_2O in the hydrated metal based ions given the data presented in Table 4.8. Ions with the same metal and same number of water molecules were averaged together. The binomial distribution for an 85% deuterium plasmoid was observed with ammonia containing ions.

Since the ion trap's spectra were time resolved (88 ms/spectrum), the $\%D_{raw}$ and $\%D_{binomial}$ of the ions inside the plasmoid could be separated from the ions in the "flame-like" plasma following the plasmoid. Therefore, a series of three series of time-resolved spectra were

taken at heights of 5, 10, and 15 cm and the $\%D_{raw}$ and $\%D_{binomial}$ of $H(H_2O)_2^+$, $NO(H_2O)^+$, $H(H_2O)_3^+$, and $Cu(CH_3CN)(H_2O)^+$ were calculated and tested for validity as described above. These heights (5, 10, and 15 cm) correspond to time scales of ~90, ~164, and ~224 ms after the initial discharge, respectively. The results of this analysis are summarized in Table 4.9 and Figures 4.7 and 4.8. In each trial the $\%D_{raw}$ and $\%D_{binomial}$ were calculated for both the plasmoid (the first spectrum with appreciable signal), and the flame-like plasma (all following spectra, averaged) as described in Chapter 2.3.

		Plasmoid		Flame-like Plasma	
Height	Ions	$\%D_{raw}$	$\%D_{binomial}$	$\%D_{raw}$	$\%D_{binomial}$
5 cm	$H(H_2O)_n^+$	0.70	0.82	0.74	0.82
	NO^+, Cu^+	0.67	0.81	0.73	0.88
10 cm	$H(H_2O)_n^+$	0.73	0.80	0.68	0.78
	NO^+, Cu^+	0.66	0.82	0.67	0.80
15 cm	$H(H_2O)_n^+$	0.80	0.86	0.52	0.57
	NO^+, Cu^+	0.67	0.85	0.50	0.56

Table 4.9 The calculated $\%D_{raw}$ and $\%D_{binomial}$ for the hydronium-based ions ($H(H_2O)_2^+$ and $H(H_2O)_3^+$, averaged) and non-hydronium based ions ($NO(H_2O)^+$ and $Cu(CH_3CN)(H_2O)^+$, averaged) at heights of 5, 10, and 15 cm in both the plasmoid and the following flame-like plasma.

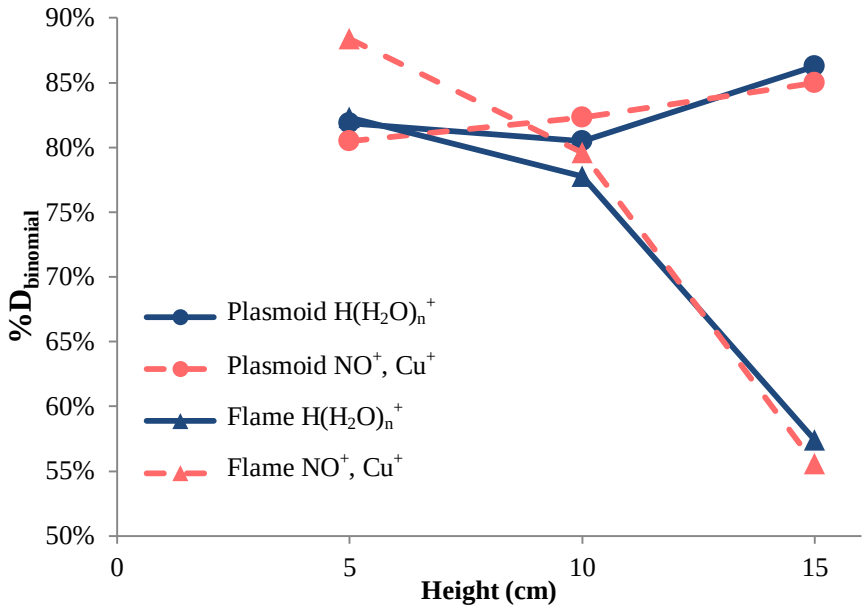

Figure 4.7 The calculated $\%D_{binomial}$ for the hydronium-based ions ($H(H_2O)_2^+$ and $H(H_2O)_3^+$, averaged) and non-hydronium based ions ($NO(H_2O)^+$ and $Cu(CH_3CN)(H_2O)^+$, averaged) at heights of 5, 10, and 15 cm in both the plasmoid and the following flame-like plasma.

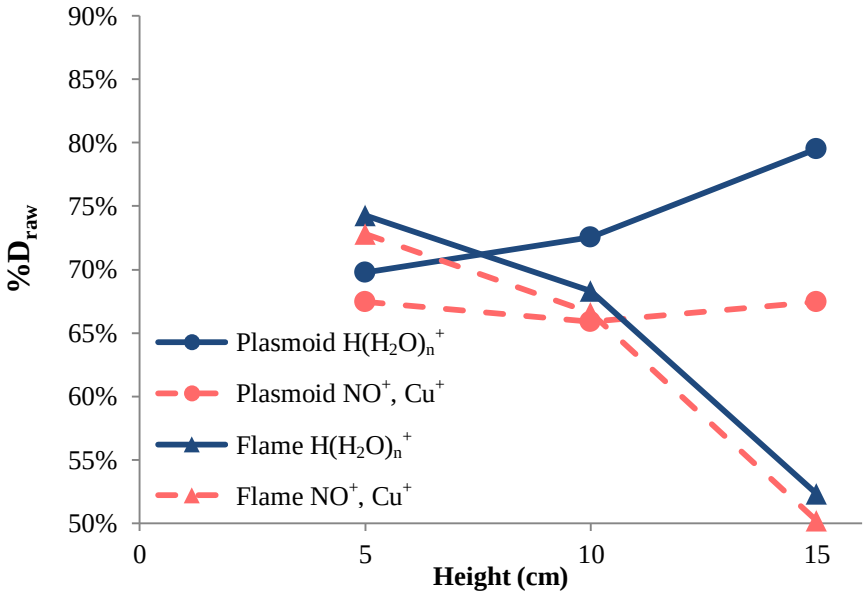

Figure 4.8 The calculated $\%D_{raw}$ for the hydronium-based ions ($H(H_2O)_2^+$ and $H(H_2O)_3^+$, averaged) and non-hydronium based ions ($NO(H_2O)^+$ and $Cu(CH_3CN)(H_2O)^+$, averaged) at heights of 5, 10, and 15 cm in both the plasmoid and the following flame-like plasma.

Results and Discussion

In *Plasma Chemistry* [30], Fridman describes how water-based plasmas with low-temperature electrons (T_e < 1eV) can dissociate water molecules via vibrational excitation (Reaction 4.1) followed by a collision (Reaction 4.2), or by dissociative attachment (Reaction 4.3) followed by electron detachment (Reaction 4.4). Both of these mechanisms produce the H and OH observed in the plasmoid [16] [19]. These products must then eventually recombine with themselves or with each other, producing H_2, H_2O_2, or H_2O. H_2 and H_2O_2 both easily react at high temperatures, eventually forming H_2O.

Reaction 4.1. $H_2O + e^- \rightarrow H_2O^* + e^-$

Reaction 4.2. $H_2O^* + H_2O \rightarrow H + OH + H_2O$

Reaction 4.3. $H_2O + e^- \rightarrow H^- + OH$

Reaction 4.4. $H^- + e^- \rightarrow H + 2e^-$

Since the recombination of H and OH is blind to the isotope, one would expect that a plasma with a mixture of D_2O and H_2O and a reasonable electron density would eventually display a binomial distribution of hydrogen and deuterium atoms. Similarly, hydration and dehydration reactions involving the isotopologues of H_3O^+ and H_2O and D_2O would eventually produce the same distribution. In contrast, if H_2O were introduced into the plasmoid after the electron and ion densities were insignificant, these hydrogen atoms would not mix well with deuterium. With this mental framework, one can interpret the stark differences between $\%D_{binomial}$ and the $\%D_{raw}$ of the plasmoid vs. the flame-like plasma that follows the plasmoid (discussed in Chapter 2.3).

The most obvious trend in Figure 4.7 is the much larger $\%D_{binomial}$ in the plasmoid compared to the flame-like plasma at longer times. As Figure 4.7 shows, the $\%H_{binomial}$ in the

flame-like plasma at 15 cm is 3 times as large as the plasmoid's $\%H_{binomial}$. This additional hydrogen added in the flame-like plasma, is presumably from the atmospheric humidity entering the plasma as it rises. This observation confirms that the structure of the plasmoid protects the plasma inside itself from the ambient air much more effectively than a structure-less plasma in which the air's humidity freely mixes with the plasma and therefore freely exchanges its protons with the deuterated water, especially at higher heights.

There are two other interesting side-notes about the $\%D_{binomial}$. First the plasmoid's $\%D_{binomial}$ increases as it rises. This could be a result of D_2O evaporating from the aqueous solution over the course of the entire trial, and progressively being drawn into the plasmoid. In contrast, the hydrogen atoms that are mixed with deuterium in the plasmoid presumably come from humidity in the air near the surface of the aqueous solution while the streamers and plasmoid are first forming. As D_2O evaporates and the plasma heats up, the surrounding air and humidity will be displaced from the vicinity of the plasma, preventing more H_2O from being added to the plasma. This exclusion of additional hydrogen and incorporation of additional deuterium into the plasmoid as it rises would produce a larger $\%D_{binomial}$ for the plasmoid at higher heights.

The second curious observation is that the $\%D_{binomial}$ of the non-H_3O^+ based ions in the flame-like plasma is higher than that of plasmoid's at 5 cm. The cause for this disparity is not entirely clear; however it might be due the difference between the geometry of the flame-like plasma versus the plasmoid. These NO^+ and Cu^+ based ions presumably form at the central electrode because copper is present there, and because the hottest electrons are presumably at the central electrode, which are required to form NO^+ from N_2 and O_2. Due to lack of a flow structure in the flame, diffusion should be the primary means of transport, meaning it takes some

time for the inner NO^+ and Cu^+ based ions to reach the hydrogen species arriving from the atmosphere. Furthermore, in the discharge, some D_2O is evaporated, making the atmospheric humidity partially deuterated already. Apparently, the diffusion of D and OD is not complete by the time the flame is at 5 cm, but is complete at10 cm. In contrast to the flame, the plasmoid appears to behave like a toroidal vortex [26] and it does have a structure that actively mixes its contents, meaning one would expect all the ions to have the same $\%D_{binomial}$.

When comparing the $\%D_{binomial}$ to the $\%D_{raw}$, the same basic trend is observed, however the $\%D_{raw}$ is typically ~10% lower. Specifically, of all the hydrogen atoms observed, 51% of those in the plasmoid and 35% of those in the flame-like plasma were extra, non-randomized H_2O (see Figure 4.6 for visualization). There are two phenomenological explanations for the source of the large amount of non-randomized H_2O: humidity in the air, or water in the capillary or the mass spectrometer. One would expect that if this H_2O originated in the air, the mass spectrum would reveal that the amount of H_2O in the plasma would increase with capillary height since it has more time to mix, producing a lower $\%D_{raw}$ at higher heights. In contrast, if the H_2O were introduced inside the mass spectrometer or capillary, one would expect the amount of H_2O to stay relatively constant with capillary height.

As is seen in Figure 4.8, the amount of non-randomized H_2O in the plasmoid clearly does not increase as the plasmoid rises. In fact the amount of H_2O attached to the hydronium based ions in the plasmoid actually decreases by a factor of 33% from 5 cm to 15 cm, strongly suggesting that the non-randomized H_2O comes from the mass spectrometer. The reason the non-hydronium based ions in the plasmoid do not follow the same pattern is unclear, however it may be because there are free $Cu(CH_3CN)^+$ and NO^+ ions in the plasmoid, making them more available for hydration in the capillary or mass spectrometer than the unobserved H_3O^+.

A final conclusion that can be drawn from the ratio of hydrogen to deuterium is the amount of H_2O that appears to be added in the mass spectrometer, and therefore is not representative of the conditions in the plasmoid. This can be corrected by calculating the percent of each ion's signal in the mass spectrum that is accounted for by a binomial distribution of hydrogen and deuterium, called the %Randomized. In practice this was done by solving for the amount of un-mixed H_2O added to an ion's signal [H_2O_{added}] using the following equation in which [D_2O] and [HDO] are the normalized concentrations in the binomial model described by $\%D_{binomial}$.

$$\%D_{raw} = \frac{[D_2O] + \frac{1}{2}[HDO]}{1 + [H_2O_{added}]}$$

From the calculated H_2O_{added}, the %Randomized was calculated according to the following formula:

$$\%Randomized = \frac{1}{1 + [H_2O_{added}]}$$

This value represents the percent of each hydrated ion that is thought to have been present in the plasmoid before additional hydration occurred with H_2O in the capillary and mass spectrometer. This calculation assumes that the plasmoid had a binomial distribution of hydrogen and deuterium before entering the mass spectrometer. Table 4.10 is generated from these results.

Height	Ions	% Randomized
5 cm	$H(H_2O)_n^+$	85%
	NO^+, Cu^+	84%
10 cm	$H(H_2O)_n^+$	90%
	NO^+, Cu^+	80%
15 cm	$H(H_2O)_n^+$	92%
	NO^+, Cu^+	79%

Table 4.10 The percent of each ion's signal in the plasmoid's mass spectrum that is characterized by the binomial distribution.

4.4 Relative Ion Ratios at Different Heights and Voltages

In order to determine the relative concentrations of the consistent low-mass ions in the plasmoid, a series of 15 plasmoids were produced using a 4kV, 873μF discharge through a tungsten electrode into Bowl B, containing an HCl solution with a conductivity of 200-300 μS. Mass spectra of these plasmoids were measured with the ion trap (15-200 m/z) at capillary heights of 6, 10, 15, 17, 20, and 25 cm above the surface of the central electrode. These heights correspond to times of 90, 141, 205, 231, 269, and 333 ms, respectively. In order to only measure the mass spectrum of the plasmoid itself, not the flame-like plasma following it, only the first spectrum containing substantial signal was used. Figure 4.9 shows the amount of each ion relative to the total signal observed in each trial. Figure 4.10 shows the same data after it was corrected by multiplying each hydrated ion by the %Randomized presented in Table 4.10 and adding the difference to the less hydrated ion in the plasmoid, thereby account for hydration occurring within the mass spectrometer. The other ions which accounted for the majority of the ions at higher heights were primarily hydrocarbons such as $C_4H_9^+$, $C_3H_8OH^+$, $C_6H_9^+$, $C_7H_{11}^+$, $C_5H_{10}NO^+$, $C_6H_{12}NO^+$, and $C_7H_{18}N^+$.

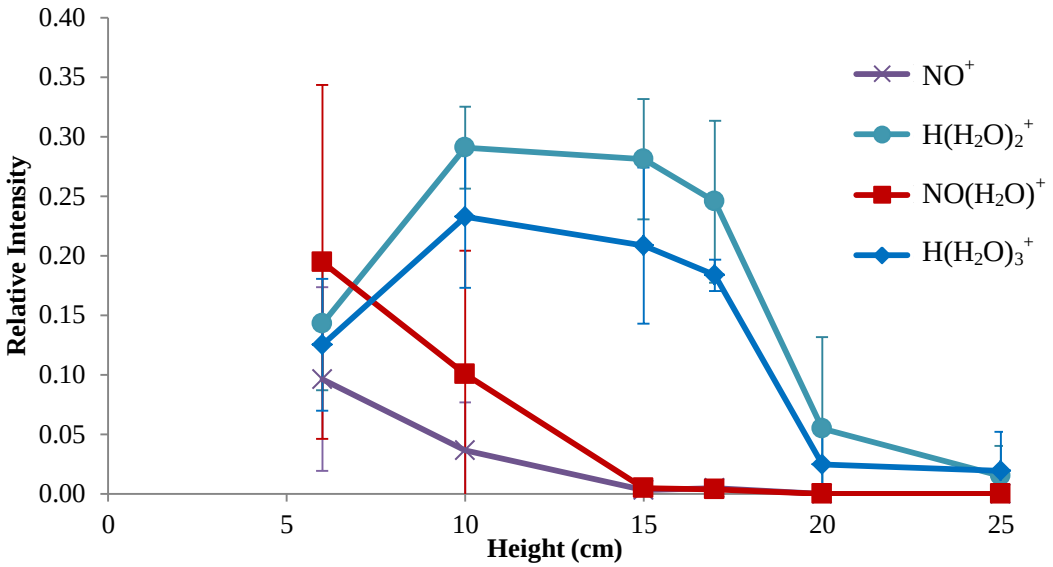

Figure 4.9 The intensity of each ion in the plasmoid relative to the total observed signal in the mass spectrum (m/z = 15-200). The error bars are one standard deviation.

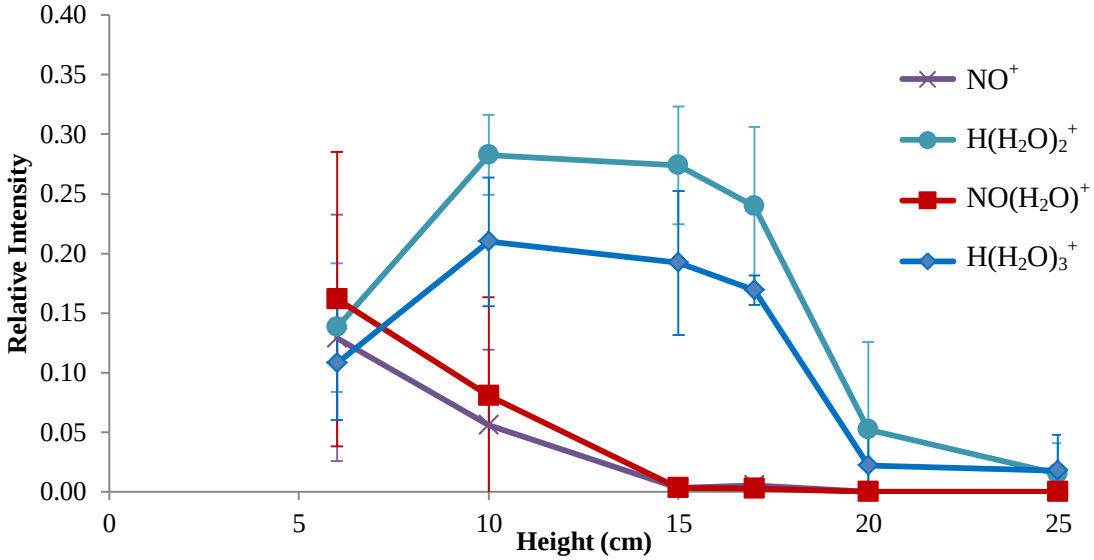

Figure 4.10 The corrected intensity of each ion in the plasmoid relative to the total observed signal in the mass spectrum (m/z = 15-200). The error bars are one standard deviation.

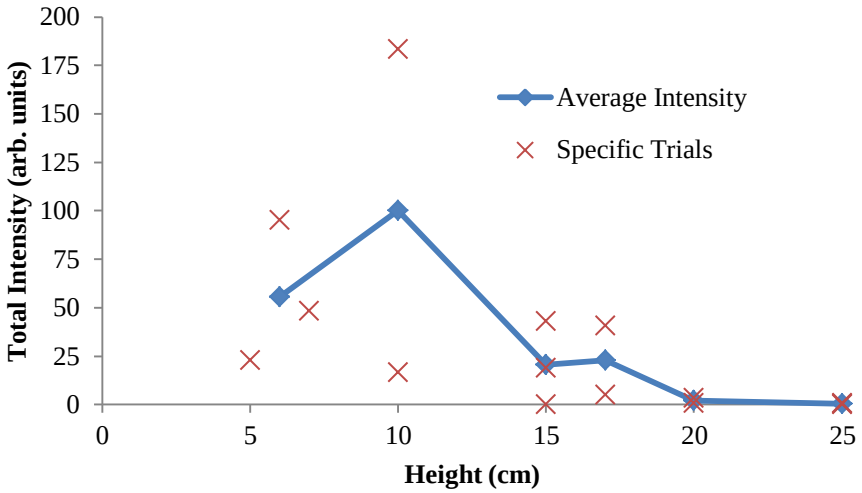

Figure 4.11 The average total intensity of ions observed in the plasmoid at several capillary heights. Error bars represent one standard deviation.

As is readily apparent from the error bars in these spectra and the total intensity of ions presented in Figure 4.11, the shot-to-shot variability in the total ion signal and the ratios of the ions was very large, especially at low heights. However, despite this variability, several clear patterns emerge from the data. First, total intensity of protonated water clusters in the plasmoid appears to be relatively constant between 10 and 17 cm (141–231 ms). This is in sharp contrast to the NO^+ based ions which show a rapid decrease in relative concentration and have all but disappeared within 205 ms after the discharge is initiated. This obvious loss of NO^+ and $NO(H_2O)^+$ is partially due to it binding to various hydrocarbons, as mentioned in Section 4.2.

In order to understand how the plasmoid's chemical make-up changes with the voltage of the discharge, a series of 9 plasmoids with voltages ranging from 3-6 kV were analyzed via the ion trap. These plasmoids were produced under identical conditions to the plasmoids described above with the capillary height held at 7 cm. Figure 4.12 shows the raw and corrected ion intensities, corrected using Table 4.10, relative to the total observed intensity in each spectrum. Figure 4.13 shows the ratios of these ions relative to each other.

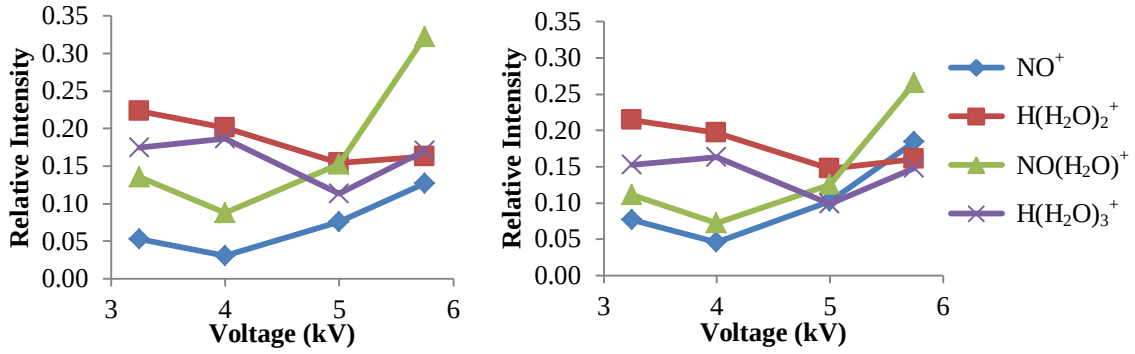

Figure 4.12 a) The intensity of each ion relative to the total signal observed in the mass spectrum. b) The corrected intensity of each ion relative to the total signal observed in the mass spectrum.

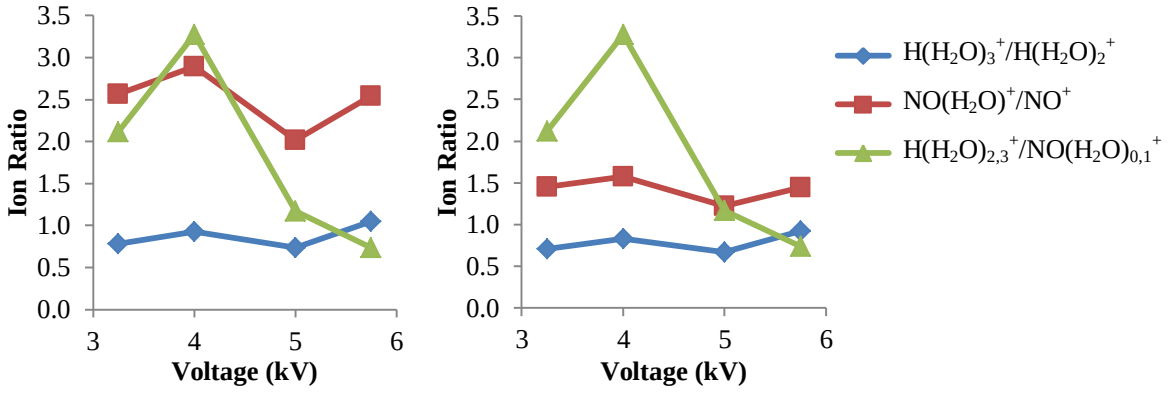

Figure 4.13 a) Selected ion ratios of the raw data presented in Figure 4.12. b) Selected ion ratios of the corrected data presented in Figure 4.13.

The results of varying the voltage revealed two significant results. The first is that higher voltages tend to produce more NO^+ based ions. The second result is that the ratios of the hydrated ions in the plasmoid do not appear to vary significantly when the voltage of the breakdown changes. Since the capillary was placed at only 7 cm from the central electrode, it appears that the temperature of the plasmoid remains constant regardless of the discharge voltage. An attempt was made at determining the plasmoid temperature based on the corrected ion ratios using pairs of hydrated and unhydrated ions, and their respective thermodynamic quantities. This appeared to be especially promising since the ratios of $H(H_2O)_3^+$ to $H(H_2O)_2^+$

and $NO(H_2O)^+$ and NO^+ followed the same trend in Figure 4.13. However, the temperatures calculated from these and other pairs of ions in the orbitrap were very inconsistent, ranging from 900 K – 2000 K. These results could be due to temperature variability between trials or, for the ion pairs observed in the orbitrap, different amounts of ions originating in the flame-like plasmoid, which could have different temperatures as well. Regardless of the cause, these results do hint that the gas temperature of the plasmoid is hotter than basic buoyancy calculations predicted based off the velocity of the plasmoid.

REFERENCES

[1] Egorov, A.; Stepanov, S. *Technical Physics* **2002**, *47*, 1584–1586.

[2] Sergeichev, K.; Lukina, N.; Fesenko, A. *Plasma Physics Reports* **2013**, *39*, 144 – 154.

[3] Xuexia, P.; Zechao, D.; Pengying, J.; Weihua, L.; Xia, L. *Plasma Science and Technology* **2012**, *14*, 716.

[4] Sakiyama, Y.; Graves, D. B.; Chang, H.-W.; Shimizu, T.; Morfill, G. E. *Journal of Physics D: Applied Physics* **2012**, *45*, 425201.

[5] Tendero, C.; Tixier, C.; Tristant, P.; Desmaison, J.; Leprince, P. *Spectrochimica Acta Part B: Atomic Spectroscopy* **2006**, *61*, 2 – 30.

[6] Xi, C.; Pan, W.; Meng, X.; Cheng, K.; Xu, D.; Wu, C. *Pure Appl. Chem.* **2006**, *78*, 1253–1264.

[7] Hayashi, N.; Satomi, H.; Kajiwara, T.; Tanabe, T. *Electrical and Electronic Engineering, IEEJ Transactions on* **008**, *3*, 731–733.

[8] Stephan, K. D.; Dumas, S.; Komala-Noor, L.; McMinn, J. *Plasma Sources Science and Technology* **2013**, *22*, 025018.

[9] Friday, D. M.; Broughton, P. B.; Lee, T. A.; Schutz, G. A.; Betz, J. N.; Lindsay, C. M. *The Journal of Physical Chemistry A* **2013**, *117*, 9931–9940.

[10] Egorov, A. I.; Stepanov, S. I.; Shabanov, G. D. *Physics - Uspekhi* **2004**, *47*, 99–101.

[11] Khorunzhiy, M.; Kuleshov, A.; Yefimov, B. *Plasma Science, IEEE Transactions on* **2011**, *39*, 2648 –2649.

[12] Shabanov, G.; Krivshich, A.; Sokolovski, B.; Zherebtsov, O. *Plasma Physics Reports* **2009**, *35*, 611–618.

[13] Sorokin, G.; Ruzan, L.; Germanov, I. *Atmospheric and Oceanic Optics* **2011**, *24*, 301–305.

[14] Fantz, U.; Kalafat, S.; Friedl, R.; Briefi, S. *Journal of Applied Physics* **2013**, *114*, 043302.

[15] Egorov, A.; Stepanov, S. *Technical Physics* **2008**, *53*, 688–692.

[16] Versteegh, A.; Behringer, K.; Fantz, U.; Fussmann, G.; Jüttner, B.; Noack, S. *Plasma Sources Science and Technology* **2008**, *17*, 024014.

[17] Noack, S.; Versteegh, A.; Jüttner, B.; Fussmann, G. *AIP Conference Proceedings* **2008**, *993*, 129–132.

[18] Shabanov, G.; Sokolovskii, B. *Plasma Physics Reports* **2005**, *31*, 512–518.

[19] v. Wurden, C.; Wurden, G. *Plasma Science, IEEE Transactions on* **2011**, *39*, 2078 –2079.

[20] Szklarczyk, M.; Kainthla, R. C.; Bockris, J. O. *Journal of The Electrochemical Society* **1989**, *136*, 2512–2521.

[21] Meshcheryakov, O. Wing Ltd Company, Odessa, Ukraine. Personal communication, 2013.

[22] Paiva, G. S.; Pavão, A. C.; Alpes de Vasconcelos, E.; Mendes, O.; Felisberto da Silva, E. *Phys. Rev. Lett.* **2007**, *98*, 048501.

[23] Sakawa, Y.; Sugiyama, K.; Tanabe, T.; More, R. *Plasma and Fusion Research* **2006**, *1*, 039.

[24] Turner, D. J. *Philosophical Transactions: Physical Sciences and Engineering* **1994**, *347*, 83–111.

[25] Shevkunov, S. *Doklady Physics* **2001**, *46*, 467–472.

[26] Versteegh, A. A. Analysis of a Long Living Atmospheric Plasmoid. Master Thesis, Technische Universiteit Eindhoven, November 2007.

[27] Perry, R. H.; Cooks, R. G.; Noll, R. J. *Mass Spectrometry Reviews* **2008**, *27*, 661–699.

[28] Burlica, R.; Kirkpatrick, M. J.; Locke, B. R. *Journal of Electrostatics* **2006**, *64*, 35 – 43.

[29] Fridman, A. *Plasma Chemistry*; Cambridge, 2008; pp 33-35.

[30] Fridman, A. *Plasma Chemistry*; Cambridge, 2008; pp 318-325.